Sorbent based Enthalpy Recovery Ventilator (SERV) in Northern Building Applications

by

Ecem Cerrah

M.Sc., Bogazici University, 2015

B.Sc., Yildiz Technical University, 2012

Thesis Submitted in Partial Fulfillment of the
Requirements for the Degree of
Master of Applied Science

in the
School of Mechatronics System Engineering
Faculty of Applied Sciences

SIMON FRASER UNIVERSITY

Spring 2019

Approval

Name:	**Ecem Cerrah**
Degree:	**Master of Applied Science**
Title:	**Sorbent based Enthalpy Recovery Ventilator (SERV) in Northern Building Applications**
Examining Committee:	**Chair:** Mohammad Narimani Lecturer
	Majid Bahrami Senior Supervisor Professor
	Gary Wang Supervisor Professor
	Woo Soo Kim Internal Examiner Associate Professor
Date Defended/Approved:	June 3, 2019

Abstract

Sorbent-based enthalpy recovery ventilator (SERV) is a potential replacement for conventional heat or enthalpy recovery ventilator (HRV/ERV) that require defrosting mechanisms in cold climates, such as in Canada. Sorbent materials (e.g. silica gel, $CaCl_2$, alumina oxide) are non-toxic, inexpensive materials. However, the bulkiness, high pressure drop and large mass of adsorbent are major disadvantages of SERV in packed bed form.

In this study, a novel design of sorbent discs with air channels is investigated which feature high heat and mass transfer performance with low pressure drop. A theoretical model is developed for heat and mass transfer in air channels in sorbent discs. A sensitivity analysis performed on design parameters e.g. channel diameter and spacing to achieve an optimum design. A prototype SERV is built in our laboratory. A custom-made experimental set-up equipped with thermocouples, humidity sensors, and an orifice plate air flow meter is designed based on ASHRAE 84 standards to evaluate the performance of the SERV prototype. The performance of the SERV is evaluated for several air flow rate, cycle time and outdoor air temperatures down to -15°C. It is shown that the proof of concept SERV consisting of 2.5 kg of heat storage materials and 2.1 kg of active sorbent material can recover up to 70% of heat and 80% of moisture from exhaust air (up to 20 CFM). It corresponds to 103 W of heat and 43 g of moisture recovery per hour which is comparable to the packed bed sorbent system reported in the literature, however, the proposed SERV offer a 60% less pressure drop.

Keywords: Heat recovery ventilators (HRV); energy recovery ventilators (ERV); passive house; green buildings; adsorption; desiccant dehumidification, heat and mass transfer; interrupted boundary layer

Acknowledgements

I would like to thank my senior supervisor, Dr. Majid Bahrami, for his support, providing an excellent research facility with all the necessary equipment and chances to get my hands dirty.

I am also thankful to my supervisory committee members, Dr. Woo Soo Kim, and Dr. Gary Wang for their time reading my thesis and their constructive comments.

I would like to thank my colleagues at Laboratory for Alternative Energy Conversion at Simon Fraser University and past members Dr. Wendell Huttema and Marius Haiducu for their support, contribution and all the fun times.

I would like to especially thank Dr. Claire McCague not only for her technical expertise in the chemical part of my project but also for being a great mentor to me.

I would like to thank all my friends for walking with me through this journey, sharing all the great moments to be remembered.

Finally, I would like to thank my parents, sister and all my family for their unconditional love, support and encouragement throughout my life. Special thanks to my dear niece, Lara, for cheering me up all the time.

Table of Contents

Approval i
Abstract ii
Table of Contents iii
List of Tables vi
List of Figures vii
Glossary x
Executive Summary xiii

Chapter 1. Introduction 1
1.1. Key technologies for heat and moisture recovery ventilation in northern climates 4
1.2. Heat and moisture recovery ventilation system performance indicators 7
1.3. Objectives and methodology 9
1.4. Literature review 10
1.4.1. Heat and mass transfer modeling in air channels with sorbent walls 12
1.4.2. Heat and mass transfer in developing boundary layer region 14

Chapter 2. Theoretical modeling 16
2.1. Heat and mass transfer model 16
2.1.1. Governing equations 17
2.1.2. Heat and mass transfer coefficients 20
2.1.3. Initial and boundary conditions 25
2.1.4. Solution procedure and verification 25
2.1.5. Sensitivity analysis to design a proof of concept sorbent discs unit 28
Effect of the channel diameter to the spacing ratio (d/s) and number of the channels 29
Effect of number of discs 31
Conclusions of the sensitivity analysis 34

Chapter 3. Experimental study 35
3.1. Sorbent disc sample preparation 35
3.2. Experimental set-up 37
3.3. Test instruments and uncertainty analysis 39
3.4. Performance evaluation 41

Chapter 4. Performance analysis 45
4.1. Operational conditions parametric study 45
4.1.1. Effect of air flow rate 45
4.1.2. Effect of cycle time 48
4.1.3. Effect of outdoor air conditions 50
4.2. Performance comparison with packed bed sorption system 53

Chapter 5. Conclusions and future work 57

References 58

Appendix A. 66

Appendix B. 74

Appendix C. 80

List of Tables

Table 1 Potential energy savings of an HRV/ERV for 260 m^2 family house with 160 CFM ventilation rate [26] 4
Table 2 Summary of modeling approaches for heat and mass transfer model in desiccant channels 13
Table 3 Coefficients based on boundary conditions and channel shape [60] 22
Table 4 Test conditions for preliminary test 26
Table 5 Constant design parameters for sensitivity analysis 28
Table 6 Test instruments and uncertainties 40
Table 7 Performance parameters for the sample test 41
Table 8 Operational conditions for the experimental data 45
Table 9 Operational conditions for climate variation tests 50
Table 10 Operational conditions of the sorbent discs experiments 53
Table 11 Experimental data 66

List of Figures

Preliminary Figure 1 Research roadmap xvi

Figure 2 (a) Energy use by sector, (b) distribution of residential energy use in Canada in 2016 reported by Natural Resources Canada [2], [3] 1

Figure 3 Predicted energy demand and potential savings by sector by 2050 in Canada [21] 2

Figure 4 Climate zone map of Canada for Energy Star certification from the Canadian Model National Building Code (2010) [23] 3

Figure 5 Schematic of VENTIREG system showing the temperature and moisture fronts in heat storage and sorbent beds during exhaust and supply flow modes, t is time and $t_1 < t_2 < t_3$ [10] 6

Figure 6 Desired air conditions in an enthalpy recovery ventilation system operating in cold climate 7

Figure 7 Sorbent disc geometry 9

Figure 8 Various sorbent bed configurations a) packed bed, b) desiccant wheel with coated channels, c) composite desiccant with air channels 11

Figure 9 Velocity (u), temperature (T) and concentration (ω) profiles and related boundary layers shown for flow over a flat plate 14

Figure 10 Air side and sorbent side control volumes are shown on a unit channel of the sorbent disc 16

Figure 11 Mass balance in air and sorbent control volumes 18

Figure 12 Energy balance in air and sorbent control volumes 19

Figure 13 Nusselt number for various cross-section geometries versus aspect ratio [60], [63], [64] 22

Figure 14 Verification of model with experimental data a) VCOP, b) latent effectiveness 27

Figure 15 Variation of channel diameter a) d=2.5 mm, s=19 mm, A_s = 2.1 cm^2, b) d=5 mm, s=22 mm A_s = 1.1 cm^2, c) d=10 mm, s=27 mm, A_s = 0.3 cm^2 29

Figure 16 Latent effectiveness for channel diameter 1.5 mm to 20 mm (or diameter to space ratio (0.8 to 0.35) 30

Figure 17 VCOP for channel diameter 1.5 mm to 20 mm (or diameter to space ratio (0.8 to 0.35) 30

Figure 18 MRC^* for channel diameter 1.5 mm to 20 mm (diameter to space ratio (0.8 to 0.35) 31

Figure 19 Effect of number of discs on latent effectiveness at 10, 20 and 30 CFM air flow rates 32

Figure 20 Effect of number of discs on VCOP for 10, 20 and 30 CFM air flow rates 32
Figure 21 Effect of number of discs on MRC* for 10, 20 and 30 CFM air flow rates 33
Figure 22 Sample preparation steps 36
Figure 23 a) Schematic of the testbed showing the sensor locations, b) photo of the set -up built in our laboratory 38
Figure 24 Sorbent discs placed in an 8.5” duct with 7.5 cm spacing and sealed by a rubber seal 39
Figure 25 Air flow through the SERV unit during a) inhale, b) exhale periods 42
Figure 26 Specific humidity, ω, of outdoor air (OA) and supply air (SA) during inhale period; return air (RA) and exhaust air (EA) during exhale period 43
Figure 27 Temperature of outdoor air (OA) and supply air (SA) during inhale period; return air (RA) and exhaust air (EA) during exhale period 43
Figure 28 MRC* for various air flow rates compared against the present model, Chapter 2 46
Figure 29 VCOP for various air flow rates compared against the present model, Chapter 2 46
Figure 30 Latent effectiveness for various air flow rate compared against the present model, Chapter 2 47
Figure 31 MRC* for various half cycle times (equally timed inhale and exhale) compared against the present model, Chapter 2 48
Figure 32 VCOP for various half cycle times (equally timed inhale and exhale) compared against the present model, Chapter 2 49
Figure 33 ε_L for various half cycle times (equally timed inhale and exhale) compared against the present model, Chapter 2 49
Figure 34 MRC* for various outdoor air conditions compared against the present model, Chapter 2 51
Figure 35 VCOP for various outdoor air conditions compared against the present model, Chapter 2 51
Figure 36 Latent effectiveness for various outdoor air conditions compared against the present model, Chapter 2 52
Figure 37 Comparison of latent effectiveness of sorbent discs (SERV) to packed bed system (VENTIREG) 54
Figure 38 Comparison of VCOP of sorbent discs (SERV) to packed bed system (VENTIREG) 54
Figure 39 Comparison of MRC* of sorbent discs (SERV) to packed bed system (VENTIREG) 55

Figure 40 Comparison of pressure drop of sorbent discs (SERV) to packed bed system (VENTIREG) 55

Glossary

a	: channel height (m)
A_{cs}	: channel cross-section area (m^2)
A_s	: air sorbent interface surface area (m^2)
b	: channel width (m)
$c_{p,a}$	: specific heat of dry air (J/kgK)
$c_{p,\mathrm{d}}$	: specific heat of desiccant (J/kgK)
$c_{p,\mathrm{v}}$	: specific heat of water vapor (J/kgK)
d	: channel diameter (m)
d_h	: hydraulic diameter of the channel (m)
dz	: discrete channel length (m)
$f\,\mathrm{Re}$	: friction coefficient
h	: convective heat transfer coefficient (W/m^2K)
h_m	: convective mass transfer coefficient (kg/m^2s)
k_a	: thermal conductivity of the air (W/mK)
L	: length of the channel (m)
Le	: Lewis number
$\dot{m}$	: mass flow rate / mass flux (kg/s)
M_{des}	: mass of desiccant in one channel (kg)
n	: number of cycles
Nu	: Nusselt number
P	: perimeter of the channel (m)
P_{fan}	: fan power (W)
P_{vs}	: saturation pressure of vapor in air (Pa)

Pr	: Prandtl number
$\dot{q}$	: heat flux (kJ/s)
Q_{st}	: adsorption heat (J/kg)
s	: spacing between air channels (m)
Sh	: Sherwood number
t	: time (s)
T	: temperature (K)
T_a	: air temperature (K)
T_d	: desiccant temperature (K)
$\dot{V}$	: volumetric flow rate (m^3/s)
u	: air velocity(m/s)
X_d	: water uptake in the desiccant ($kg_{water}/kg_{desiccant}$)

Greek letters

α	: thermal diffusivity (m^2/s)
ΔH_{ads}	: adsorption heat (J/kg)
ΔP	: pressure drop (Pa)
ε_L	: latent effectiveness
ε_S	: sensible effectiveness
ϵ	: channel aspect ratio
γ	: shape parameter
ρ_a	: air density (kg/m^3)
ρ_d	: desiccant density (kg/m^3)
ω	: humidity ratio (kg_{water}/kg_{air})
ω_{eq}	: humidity ratio at equilibrium (kg_{water}/kg_{air})

Subscripts

a	: air
d	: desiccant
eq	: equilibrium
s	: sorbent
v	: vapor
w	: water

Abbreviations

BU	: between sorbent and heat storage units
EA	: exhaust air
ERV	: enthalpy recovery ventilator
GSR	: gas side resistance
GSS	: gas and solid side resistance
HRV	: heat recovery ventilation
LAEC	: Laboratory for alternative energy conversion
MERV	: membrane based enthalpy recovery ventilation
MRC	: moisture recovery capacity (kg_w/h)
MRC*	: modified mositure recovery capacity ($kg_w/kg_s h$)
OA	: outdoor air
PGS	: pseudo gas side resistance
RA	: return air
RER	: recovery efficiency ratio
RH	: relative humidity
SERV	: sorbent based enthalpy recovery ventilation
SA	: supply air
VCOP	: ventilation coefficient of performance

Executive Summary

Motivation

At the United Nations climate change conference in Paris (COP21), Canada announced the target of reducing greenhouse gas (GHG) emissions to 30% below the emission levels in 2005, by 2030 [1]. Based on the data published by Natural Resources Canada in 2016, 17% of the energy use in Canada is related to the residential sector, responsible for 14% of national GHG emissions [2]. Space heating accounts for 61% of residential energy use [3]. Infiltration and the costs associated with that, can be significantly reduced by effective residential envelope air sealing, however, it creates a need for mechanical ventilation to maintain indoor air quality.

World's highest rate of infant hospital admissions due to respiratory infections was reported in Nunavut in northern Canada, in Alaska and Greenland [3]. Inadequate average ventilation rate per person, 20 m^3/h in 49 Nunavut houses studied during winter 2013, was indicated to be the main cause of respiratory infections [4]. The minimum ventilation rate of a living space is determined by ASHRAE standards, e.g. 75 m^3/h fresh air is required for a typical 70 m^2 single bedroom apartment [5]. Ventilation systems without heat or moisture recovery are responsible for significant energy losses. The annual total energy delivered for space conditioning in 13 developed countries, is estimated to be 19 EJ and 48 % of it is lost due to ventilation [6].

In cold climates, such as in Canada, the temperature difference between indoor and outdoor can be more than 40 °C and the moisture content of the outdoor air is low, i.e., in the range of 1 to 2 g/kg for below zero ambient temperatures. Therefore, the fresh air drawn into buildings, must be heated and humidified for human comfort per ASHRAE standards [6]. Sensible heat exchangers or enthalpy exchangers that recover both heat and moisture from the exhaust air are used to heat or humidify the incoming (supply) fresh air. Estimates show that 60-95% of the heat in exhaust air can be recovered by heat recovery systems with only the cost of fan power in the range of 2-7 W [8]. However, in very cold climate zones such as the Arctic, there are problems associated with frost formation due to relatively high humidity (high dew point temperature) in the exhaust air. During heat recovery, when the temperature of the exhaust air drops lower than its dew

point temperature, condensation happens in the air channels of the exchanger and cause frost formation at below zero temperatures. The ice formed inside the channels, can block the air flow and if not detected, it can damage the heat exchanger core. In heat exchangers, frost formation starts when the outdoor temperature drops below -5 °C. Moisture exchange in membrane based energy exchangers enable them to operate without freezing issues down to -10 °C of outdoor temperatures [9]. In extreme cold climates, e.g. below -10 °C, defrosting strategies are required to maintain the operation of heat or enthalpy exchangers. Preheating the exhaust air or recirculation of warm exhaust air are common defrosting strategies however, they reduce the effectiveness of the exchangers.

A novel enthalpy recovery ventilation system, called VENTIREG was build and tested by Aristov et al. [10] in Novosibirsk, Russia (winter temperature down to -30 °C). The device consisted of two packed beds of particles for: i) sensible heat storage (glass or lead balls of 2-4.5 mm diameter or gravel of irregular shape 4-7 mm in size), and ii) sorbent-based moisture recovery bed (silica gel, alumina or alumina impregnated with $CaCl_2$, pellet size 1.8-4.5 mm in diameter and 6-8 mm in length). This system works intermittently in exhaust and supply modes following each other in a predetermined cycle time. During exhaust mode, the warm and humid exhaust air from the indoor is first pushed through the sorbent bed releasing its moisture content to the sorbent material. Then, the air flows through the sensible heat storage bed where it is cooled down and exhausted out. Since the moisture content of the air is decreased notably (dew point temperature is decreased) in the sorbent bed, it can be cooled down to below zero degrees without frost issues. During the following supply mode, cold and dry outdoor air is pulled in and passed through the heat storage bed and sorbent bed. It is heated and humidified by recovering both heat storage and sorbent beds. Laboratory and field tests of the system demonstrated 70-90% moisture recovery and 60-96% heat recovery from exhaust to supply air streams without any frost. The system is effective and inexpensive to build however, require higher fan power compared to other ventilation systems, 20-40 W for 135 m^3/h air flow, due to pressure drop along the moisture and heat storage materials. They indicated that scaling up the system from laboratory size to real life application may lead reduced efficiencies. Therefore, appropriate mathematical models needed to design a more efficient VENTIREG system.

In summary, membrane-based heat and moisture recovery ventilation systems are prone to frost problem in cold climates and need defrosting strategies that make the systems complicated and reduce their efficiency. VENTIREG system addresses the frost issue with a simple solution however, the packed beds for heat and moisture recovery make the system bulky and hard to scale up. A compact design with heat and mass transfer enhancements would make the VENTIREG system suitable for real life applications. This proposed research study focuses to understand the heat and mass transfer mechanisms between air and sorbent materials through theoretical, experimental studies and investigate possible enhancements in VENTIREG design. As an outcome, we aim to design a compact sorbent design using discs to improve heat and moisture recovery in extreme cold climate conditions (below -10°C).

Objective

The objective of this research is to design, fabricate and test a proof of concept sorbent-based enthalpy recovery ventilation (SERV) system for northern residential units (outdoor temperature below -10°C). Following research questions addressed to build a compact and efficient (minimum 60% effectiveness) SERV system:

i. How does the enhanced heat and mass transfer in entrance flow region effect performance of SERV system?

ii. How is the performance of the sorbent disc design compared to packed beds?

iii. What is the effect of sorbent disc geometry, material properties and operating conditions on the heat and mass transfer performance?

Methodology and Contributions

To achieve the objective of this program, a systematic approach is undertaken. Preliminary Figure 1 shows the roadmap of the research program. The following highlights the milestones and the steps of the methodology:

- Development of a mathematical model to accurately predict the outlet conditions of air passing through the air channels in disc-type consolidated sorbent composite [11].

- Investigation of the effect of heat and mass transfer in developing boundary region on the performance of the system [12], [13]
- Sample preparation and experimental study of air channeled composite sorbent discs for proof of concept demonstration and model verification [13], [14].
- Building a custom-designed testbed based on ASHRAE Standard 84 [15] to enable measuring the humidity and heat recovery performance of the SERV [12], [16].
- Parametric study on the operating parameters, i.e. cycle time and air flow rate and design parameters to achieve high de/humidification performance with low pressure drop [12], [16].

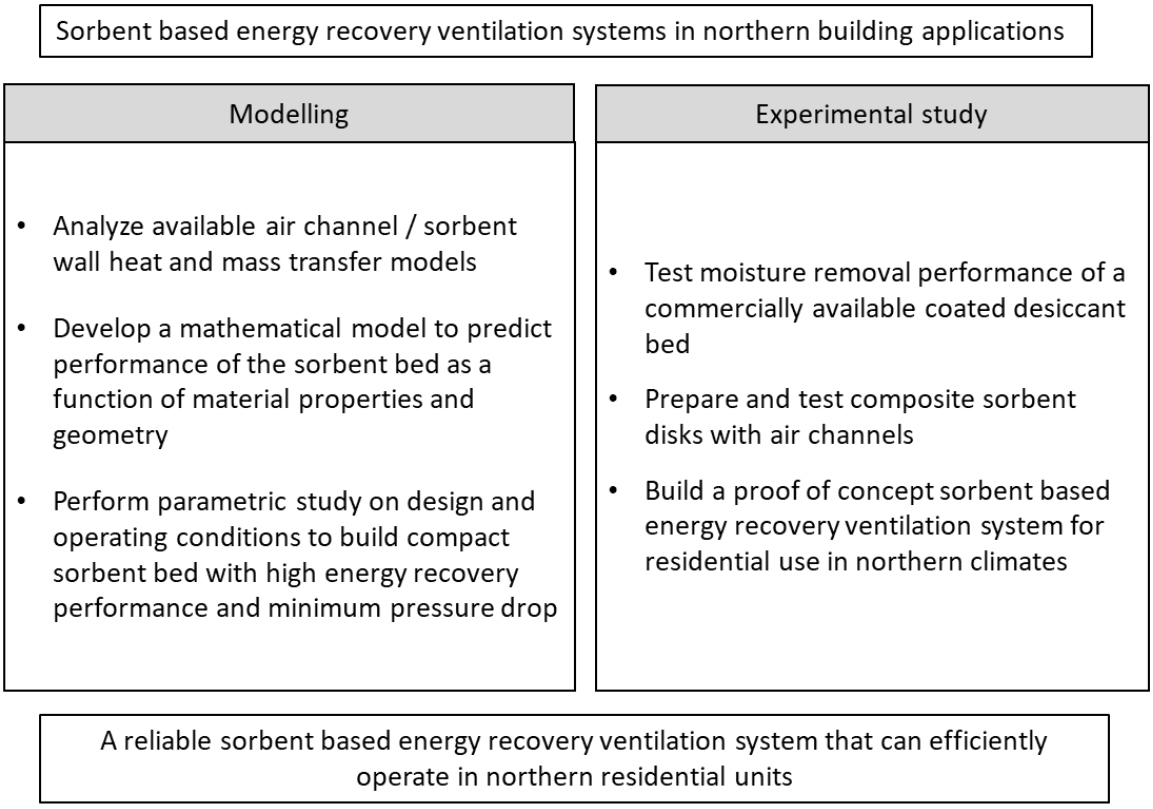

Preliminary Figure 1 Research roadmap

Publications

[11] E. Cerrah and M. Bahrami, “Optimum Performance Definition for Desiccant Wheel Systems,” in *Innovative Materials for Processes in Energy Systems (IMPRES)*, 2016, pp. 102–103.

[12] E.Cerrah and M.Bahrami, “ Performance Evaluation of a Novel Sorbent Based Enthalpy Recovery Ventilator in Northern Climates”, in preparation

[13] E. Cerrah, C. Mccague, and M. Bahrami, “Air-channel composite desiccant for northern climate humidity recovery ventilation system,” in *Heat Powered Cycles Conference*, 2018.

[14] C. Mccague, S. Shokoya, E.Cerrah and M.Bahrami,” Hygroscopic salts in porous matrices: Thermophysical properties and lab-scale testing for air conditioning applications,” in *Innovative Materials for Processes in Energy Systems (IMPRES)*, 2019 (Accepted)

[16] E. Cerrah and M.Bahrami, “A Novel Sorbent Based Enthalpy Recovery Ventilator,” *Submitt. to Pacific Rim Thermal Engineering Conference (PRTECH2019)*.

Chapter 1. Introduction

During recent decades the environmental impact of buildings on global energy demands and consequently on greenhouse gas (GHG) emissions has been increased. Building sector accounts for over 40% of global energy consumption and 18% of GHG emissions [17]. Mostly due to increasing energy demand of the developing countries, global energy demand of the buildings is predicted to grow from 145 EJ in 2013 to 243 EJ by 2050 [18], [19]. International Energy Agency (IEA) estimates about 83 EJ potential energy saving can be achieved in building sector [19].

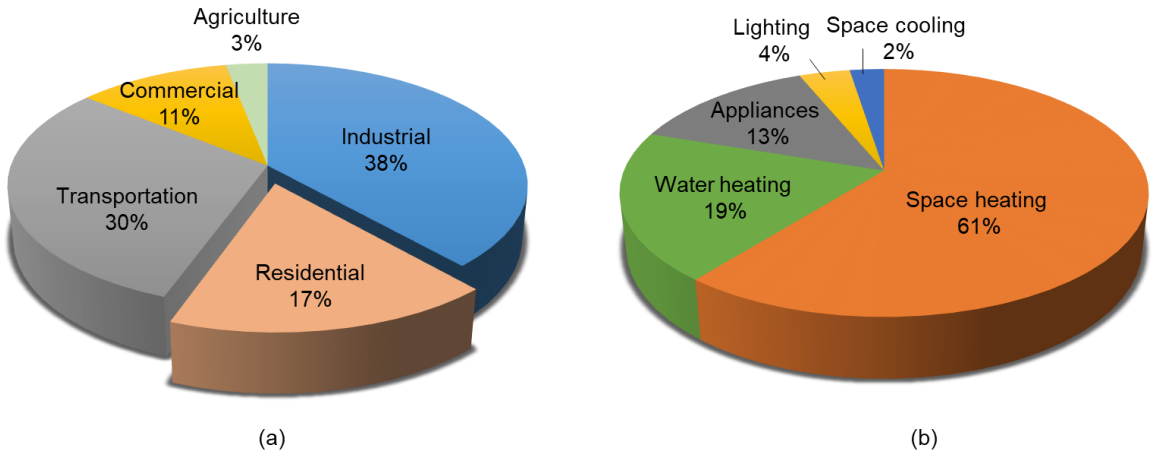

Figure 2 (a) Energy use by sector, (b) distribution of residential energy use in Canada in 2016 reported by Natural Resources Canada [2], [3]

Given the impacts that buildings have on energy consumption and GHG emissions, governments across the world are deploying strategic plans to increase energy efficiency in buildings [20]. Canada announced the 2030 target for reducing GHG emissions to 30% below the emission levels in 2005 [1]. Residential sector contributes to 14% of the national GHG emissions. As shown in Figure 2, residential sector accounts for 17% of the total energy consumption in Canada in 2016 and 61% of it is due to space heating [2], [3].

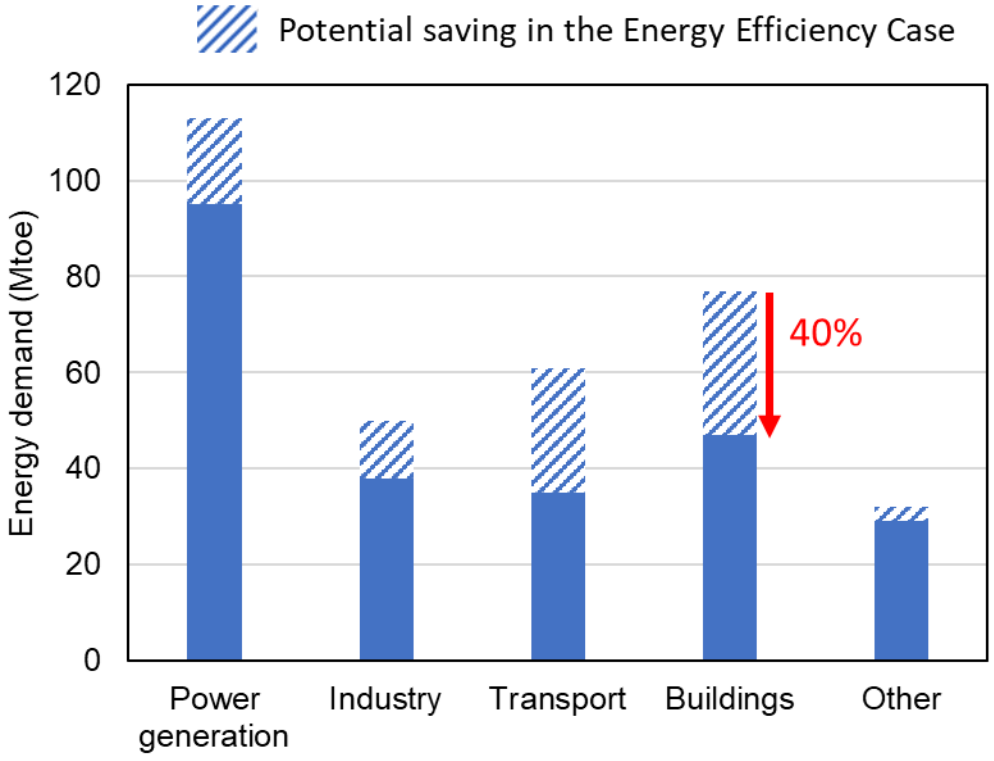

Figure 3 Predicted energy demand and potential savings by sector by 2050 in Canada [21]

International Energy Agency (IEA) predicts that energy demand in Canada will increase from 292 million tonnes of oil equivalent (Mtoe) in 2016 to 364 Mtoe in 2050 with the current standards and policies. As shown in Figure 3, the largest potential saving, 40%, is suggested for building sector by improving the air tightness, insulation, supporting renewable heating methods such as heat pumps where applicable and more stringent standards for energy efficiency of the household appliances [21].

Comprehensive building certification systems such as LEED (Leadership in Energy and Environmental Design), BREEAM (Building Research Establishment Environmental Assessment Methodology), Passivhaus, Energy Star, etc. were offered by different organizations in different countries with the emphasis on energy, environment, ecology and environment principles [22]. Building codes are usually written based on climate classifications determined by heating degree days (HDD) and cooling degree days (CDD). One HDD 18°C indicates a day during which the indoor temperature (18°C) is 1°C higher than the outdoor. The higher the HDD, the colder the climate. Figure 2 shows

climate zones in Canada based on Energy Star certification used in Canada Model National Building Code (2010) [23]. British Columbia being in the warmest zone, all provinces in Canada are in heating climate zones. Canada Model National Building Code is not enforced by law, some provinces such as British Columbia, Ontario, Quebec and Alberta, develop their own codes based on the National code.

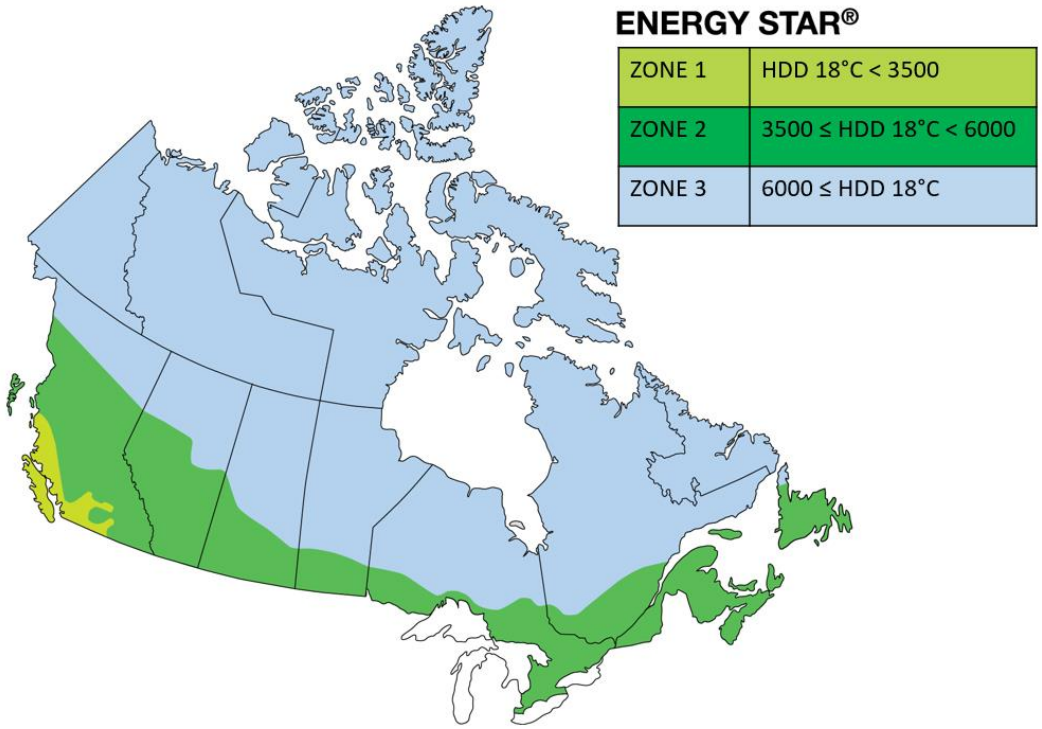

Figure 4 Climate zone map of Canada for Energy Star certification from the Canadian Model National Building Code (2010) [23]

Infiltration and the costs associated with that, can be reduced by effective residential envelope air sealing, however it creates a need for mechanical ventilation to maintain indoor air quality [24]. Building codes are based on “build tight, ventilate right” motto seeking for greater air tightness in the building envelope and higher standards for enthalpy recovery ventilators.

Energy saving strategies especially in northern climates, recommend air tight building construction and improved thermal insulation [6], [18], [24]. Reduced infiltration and natural ventilation rates raise problems due to insufficient ventilation. The highest rate of infants suffer from respiratory infections are in Northern Canada, Alaska and Greenland.

A medical study performed in Nunavut (Northern Canada) during 2013 winter, indicates the main cause of respiratory infections as the inadequate ventilation rate (~20 m^3/h) [4]. Minimum ventilation rate based on the size of living spaces and occupancy, is determined by ASHRAE standards, i.e. 75 m^3/h for a 70 m^2 single bedroom apartment [25]. Ventilation in cold climates account for 48% of the energy delivered for space heating in 13 develop countries [6].

An energy analysis completed by BC Housing Branch in Canada to investigate the potential energy savings by heat recovery in six locations across Canada representing different climate zones [26]. A typical 260 m^2, 3 bedrooms family house with continuous ventilation of 160 CFM was chosen for the analysis. The results shown in Table 1, represents the potential energy saving due to HRV/ERV system. As seen, significant energy savings can be achieved by installing HRV /ERV systems in various climates across Canada, with higher potential in colder regions.

Table 1 Potential energy savings of an HRV/ERV for 260 m^2 family house with 160 CFM ventilation rate [26]

Location	Heating Degree Days	% Reduction in Annual Heating and Cooling Energy due to HRV / ERV	
		Gas furnace & Central air conditioning	Electric baseboard & No cooling
Vancouver	2825	48%	40%
Toronto	3520	47%	41%
Montreal	4200	50%	44%
Winnipeg	5670	50%	44%
Fort McMurray	6250	54%	47%

1.1. Key technologies for heat and moisture recovery ventilation in northern climates

Ventilation in northern climates, such as most of Canada, Russia, Northern Europe and Northern states of the US is challenging due to high temperature difference between indoor and outdoor (up to 60°C), the low moisture content of the outdoor air, i.e., in the

range of 1 to 2 g/kg for below zero ambient temperatures. In order to keep the indoor human comfort per ASHRAE standards [6], the fresh air (supply air) fed in the building should be heated and humidified. To reduce the heating cost, heat recovery ventilation systems (HRVs), i.e. air to air heat exchangers can be used to recover the heat from exhaust air to supply air. HRVs can recover 60-95% of the heat depending on the heat exchanger performance and climate conditions [8]. In cold climates (below 0°C), the energy savings are more significant however, limitations exist for HRV operation due to relatively high dew point, in other words high moisture content of the exhaust air. Typical winter indoor air condition is about 18-24 °C and 40-55% RH corresponds to 5-10°C dew point temperature [7]. Therefore, frost formation starts inside the channels of the heat exchanger when the air temperature at the exhaust outlet drops down to the outdoor temperature that is much below exhaust air dew point temperature. The ice formed inside the channels can block the air flow and if not detected, it can damage the heat exchanger core.

Sorbent or membrane based enthalpy recovery ventilation systems (ERVs) that recover both heat and moisture from the exhaust air, operate with a lower frosting limit compared to conventional HRVs [27]. Beattie et al. [9] tested a polypropylene based HRV, a polymerized paper based ERV and two different membrane type ERVs (provided by dpoint Technologies) with outdoor temperatures between -5 to -35°C. In all tested systems frost problem was observed at operation below -10°C outdoor temperature. They reported 20% to 30% of air flow reduction due to ice formation in membrane based ERVs and HRV after 2 hours of operation. With factory set defrost strategy HRV had the highest sensible effectiveness (~0.84) and the ERVs had about 0.76-0.78. Latent heat transfer effectiveness was 0.61 for the polymerized paper based ERV and 0.46 and 0.52 for membrane based ERVs at -25°C outdoor temperature. At extreme cold climates (below -10°C) potential for energy savings due to heat recovery increases; however need for a defrost mechanism costs an energy penalty and complexity.

Recently a novel enthalpy recovery ventilation system named VENTIREG [10], build and tested in Novosibirsk, Russia (winter temperature down to -30 °C). In this system heat recovery and moisture recovery are performed by separate packed beds consist of sorbent material, i.e. silica gel, alumina and alumina impregnated with $CaCl_2$ (pellet size

1.8-4.5 mm in diameter and 6-8 mm in length) and heat storage material, i.e. glass balls, lead balls (of 2-4.5 mm diameter) or gravels (irregular shape 4-7 mm in size).

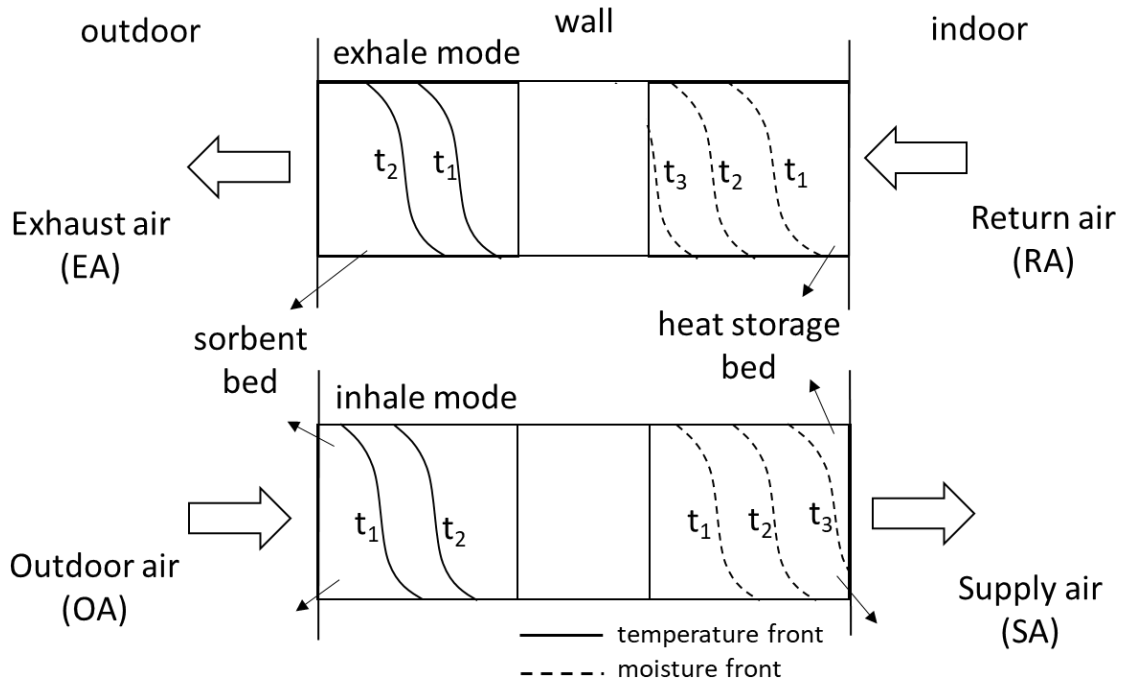

Figure 5 Schematic of VENTIREG system showing the temperature and moisture fronts in heat storage and sorbent beds during exhaust and supply flow modes, t is time and $t_1 < t_2 < t_3$ [10]

A schematic of the intermittently operating system is shown in Figure 4, in which exhale and inhale air streams are flown through the beds cyclically. In exhale mode, warm and humid air from indoor is pushed through the sorbent bed in which it releases its moisture content and its temperature increases due to exothermic sorption process. Then heat storage bed captures heat from the air before it is exhausted to outside. In the following inhale process, cold and dry air from outdoor environment is pushed through the heat storage and sorbent beds recovering both heat and moisture so that the air supplied to the room reaches comfort conditions. Cycle times adjusted by the time temperature and moisture fronts reach to the end of heat storage and sorbent beds as seen in Figure 4. In a residential unit with 135 m^3/h air flow, 60-96% heat and 70-90% moisture recovery were achieved in field tests during 2013 winter in Novosibirsk, Russia. No frost issue was observed and only operating cost of the system is reported as 20-40 W of fan power.

1.2. Heat and moisture recovery ventilation system performance indicators

A desirable heat and moisture recovery (enthalpy recovery) ventilation system that operates in cold climate should have the following features: i) high sensible and latent heat recovery performance, ii) low fan power requirement, iii) frost resistance, iv) compactness, v) low maintenance requirement, vi) no contamination, mold or odour problems.

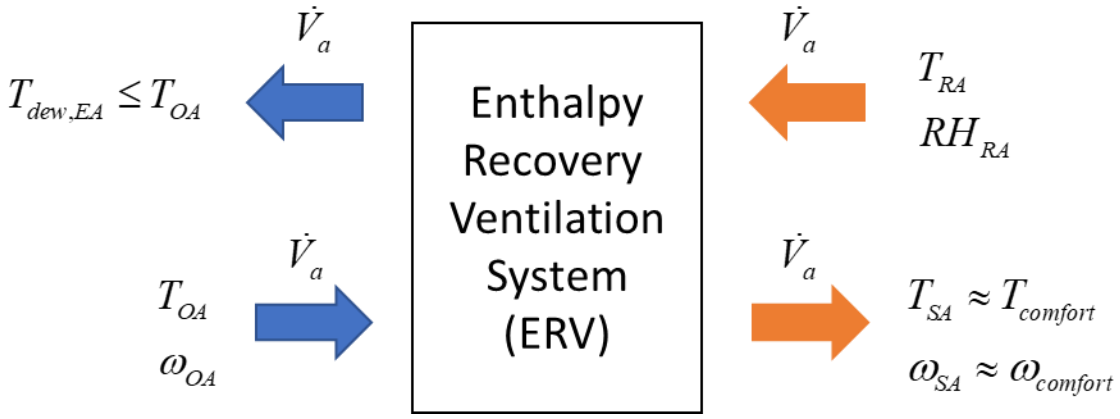

Figure 6 Desired air conditions in an enthalpy recovery ventilation system operating in cold climate

Sensible heat transfer effectiveness (ε_s, unitless) : ratio of the actual heat transfer to the maximum possible heat transfer from exhaust air to supply air [9]. εs ranges between 0 and 1. ε_s for typical heat recovery ventilators is 0.6-0.95 [8].

$$\varepsilon_S = \frac{\dot{m}_a c_{pa}\left(T_{SA} - T_{OA}\right)}{\dot{m}_a c_{pa}\left(T_{RA} - T_{OA}\right)}, \qquad 0 \le \varepsilon_S \le 1 \tag{1}$$

Latent heat transfer effectiveness (ε_L, unitless) : ratio of the actual latent heat transfer to the maximum possible heat transfer from exhale air to supply air [9].

$$\varepsilon_L = \frac{\dot{m}_a c_{pa}\left(\omega_{SA} - \omega_{OA}\right)}{\dot{m}_a c_{pa}\left(\omega_{RA} - \omega_{OA}\right)}, \qquad 0 \le \varepsilon_L \le 1 \tag{2}$$

Moisture removal capacity (MRC, kg/h): amount of moisture removal from the exhale air per hour. In a balanced system, amount of moisture removed from exhale air is equal to the amount of moisture added to the supply air.

$$MRC = \dot{m}_a \left(\omega_{SA} - \omega_{OA} \right) \tag{3}$$

In order to take both dehumidification performance and compactness into account, a new parameter MRC* (kg_w/kg_{dh}) is introduced in this study, where M_S represents the mass of the sorbent:

$$MRC^* = \frac{\dot{m}_a \left(\omega_{SA} - \omega_{OA} \right)}{M_S} \tag{4}$$

Recovery efficiency ratio (RER):

$$RER = \frac{\dot{m}_a \left(h_{SA} - h_{OA} \right)}{P_{fans} + \dot{Q}_{aux}} \tag{5}$$

Ventilation coefficient of performance (VCOP, unitless): In the literature performance of enthalpy recovery ventilation systems are measured by the parameters given above. To our knowledge, there is a lack of comprehensive performance parameter that accounts for enthalpy recovery and power consumption of the system as well as the deviation from comfort conditions in a single parameter. Therefore, we are proposing a new parameter, ventilation coefficient of performance (VCOP) that can be used to measure the performance of any enthalpy recovery system. It is defined as the ratio of actual sensible and latent heat recovery to the fan power and auxiliary heating power if applicable. Deviation from the comfort temperature and humidity level is also considered as a cost by expressing it as power consumption if it was covered by any other additional method.

$$VCOP = \frac{\dot{m}_a \left[c_{pa} \left(T_{SA} - T_{OA} \right) + h_{fg} \left(\omega_{SA} - \omega_{OA} \right) \right]}{P_{fans} + \dot{Q}_{aux} + \dot{m}_a \left[c_{pa} \left(T_{comfort} - T_{SA} \right) + h_{fg} \left(\omega_{comfort} - \omega_{SA} \right) \right]} \tag{6}$$

Minimum value of VCOP is zero when there is no sensible or latent heat recovery and maximum VCOP is infinity when there is no pressure drop (fan power is zero), no auxiliary heating and the supply air satisfies the comfort conditions. VCOP is different than

RER in the sense that VCOP accounts for deviation from the comfort conditions so that it provides a fair comparison of the system in different climate conditions. Enthalpy recovery systems are more useful when the difference between indoor and outdoor climates are higher, so that there is a higher VCOP potential for an effective ERV operating in such conditions.

1.3. Objectives and methodology

Challenges of ventilation in cold climates indicates need for research to design an efficient enthalpy recovery ventilation system that can operate in extreme cold climates (below -10°C) without frost issues. This research is focused on developing a sorbent based enthalpy recovery ventilation (SERV) system comprised of a sorbent based moisture recovery bed and a heat storage bed. A schematic of the sorbent geometry is shown in Figure 7.

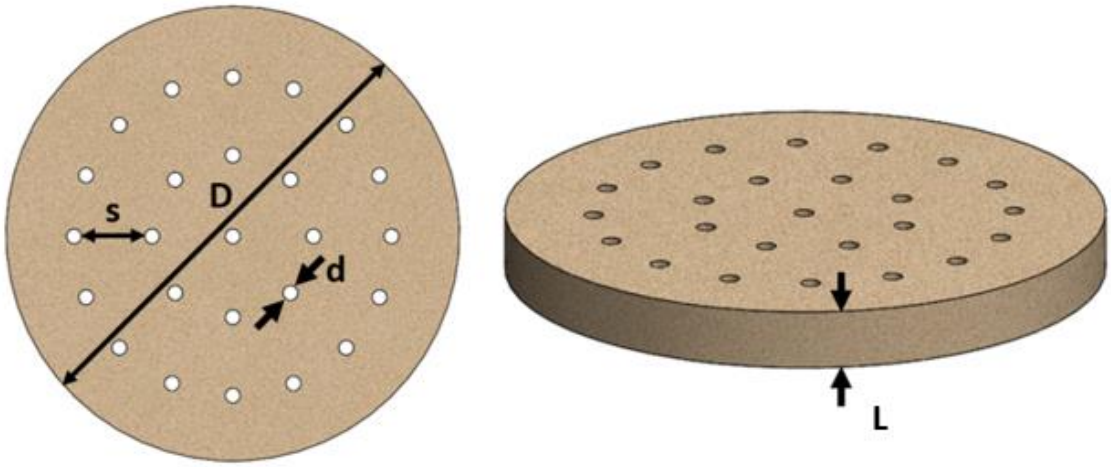

Figure 7 Sorbent disc geometry

Following research topics are studied to design an efficient enthalpy recovery system:

- Designing a number of sorbent discs to enhance the heat and mass transfer by interrupting the thermal and concentration boundary layer

- Designing air channels on the sorbent discs to create flow paths for air and reduce the pressure drop
- Investigating the heat and mass transfer in developing boundary layer for air channels surrounded with sorbent material
- Parametric study on the air channel geometry, disc geometry and arrangement for higher heat and mass transfer performance
- Selecting a suitable sensible heat storage material
- Comparing performance of the sorbent based enthalpy recovery system with other available systems, i.e. MERV, HRV in terms of sensible and latent heat effectiveness, VCOP, compactness and suitability to work in extreme cold climates

1.4. Literature review

Sorbent materials e.g. silica gel, activated carbon, zeolite have highly porous structure and high affinity to water vapor. They are commonly used for de/humidification application in air conditioning applications in tropical and subtropical climate with high humidity [28]. Wide range of particle and pore sizes allow for various sorbent bed configurations e.g. packed column of relatively large pellets, small particles coated on fibrous paper forming desiccant wheels or composite sorbent material with air channels as seen in Figure 8.

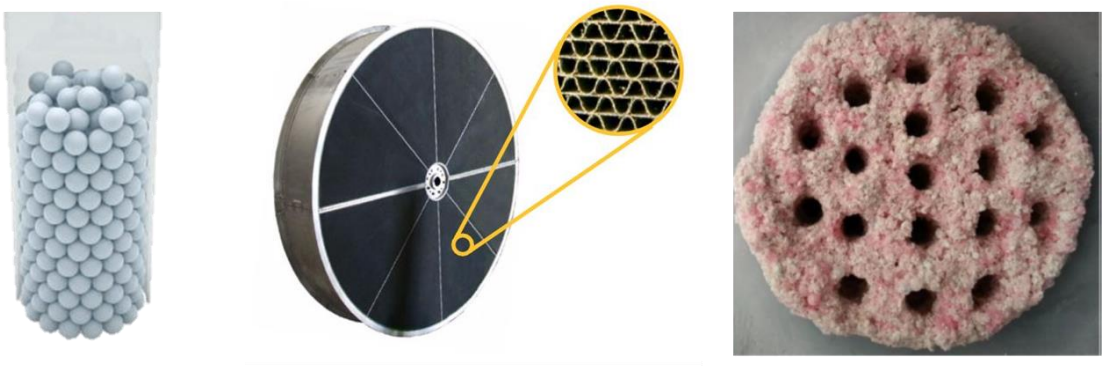

Figure 8 Various sorbent bed configurations a) packed bed, b) desiccant wheel with coated channels, c) composite desiccant with air channels

Traditional packed columns are inexpensive but cause high pressure drop. Sorbent coated sheets can be formed as sinusoidal channels, called desiccant wheel is a good alternative to bulky packed beds. However, the amount of material that is coated on desiccant wheels is limited. Although desiccant wheels have lower pressure drop compared to packed columns; small sized channels cause about 100 Pa pressure drop for 2 m/s face velocity (common design velocity) [29]. There are studies on coating of the shelf heat exchangers with sorbent material that causes lower pressure drop. However these systems are complicated as they use a refrigerant loop for removing the heat of adsorption during dehumidification and heating the sorbent for regeneration [30], [31]. These systems are not suitable for residential applications due to high maintenance, repair and replacement costs. A novel composite sorbent with air channels as seen in Figure 8c was proposed by Chen et al.[32], [33] for residential air conditioning application in order to lower the pressure drop and achieve high dehumidification performance. The composite sorbent comprise of silica gel, sodium polyacrylate and polyacrylic acid; had 40% lower pressure drop with about 35% compromise in transient dehumidification capacity. Reduction in the transient dehumidification capacity was expected as the composite desiccant has less reaction time with moisture. However, the composite sorbent had higher total adsorption capacity compared to silica gel packed column design at the same operating conditions [32]. There is no other study found for air channeled composite design. A comprehensive heat and mass transfer modeling is required to study the effect

of the geometry of the composite discs, channel size and spacing on the dehumidification performance and pressure drop.

1.4.1. Heat and mass transfer modeling in air channels with sorbent walls

Coupled heat and mass transfer inside the air channels coated with sorbent wall is a complex problem, which requires thorough knowledge about the sorbent material properties. There is a well-established literature on modeling air channels with sorbent walls for desiccant wheel channels. Many researchers have studied desiccant wheels considering simplified sets of assumptions about the coupled heat and mass transfer mechanisms. The available mathematical models are reviewed, categorized and summarized in Table 2. The existing models are categorized as gas side resistance (GSS), gas and solid side resistance (GSR) and pseudo-gas side (PGS) models. GSR includes include the detailed diffusion mechanism inside the desiccant layer. GSS models consider the desiccant layer as a bulk and takes the heat and mass transfer based on gas side resistance. PGS models take the solid side resistance into account as well, however they are adopted by lumped heat and mass transfer coefficients obtained experimentally [29].

Table 2 Summary of modeling approaches for heat and mass transfer model in desiccant channels

Modeling approach	Advantages	Disadvantages
Gas-side resistance model (GSR) [34]–[41]	• Low computation time • No need to measure the diffusivity properties of the desiccant	• Neglects mass diffusion and heat conduction within the desiccant layer
Gas and solid side resistance model (GSS)[35], [42]–[45]	• Higher accuracy due to consideration of heat and mass transfer diffusion terms	• Higher complexity and longer computation time
Pseudo-gas-side model (PGS)[46]	• Shorter computation time	• Lumped heat and mass transfer coefficients need to be obtained experimentally

Water vapor diffuses in desiccant materials by a combination of ordinary diffusion, Knudsen diffusion and surface diffusion mechanisms [29], [42]. Depending on the type of the desiccant one or more mechanism can be dominant in mass transfer. Pesaran and Mills [47] had investigated diffusion mechanisms in silica gel. They concluded that surface diffusion was the dominant mechanism for microporous silica gel, such as silica gel RD which has been mostly used as desiccant wheel material. Gas and solid side resistance models (GSS) account for diffusion terms in the mass balance of the desiccant. Worek and Sphaier [43] developed a 2D GSS model for a silica gel RD wheel, including surface diffusion and heat conduction terms across the thickness of the desiccant layer. Narayanan et al. [34] compared a 1D GSS model with a simplified gas side resistance model (GSR) in which the axial conduction and diffusion effects in the desiccant layer were neglected. They verified both models with an existing experimental study [48] and showed that for the simulated case the effect of solid side resistances was negligible. Yadav et al. [36] verified a 1D GSR model with a different set of data, which consisted of three different temperature and humidity scenarios.

After a comprehensive review of the available models in the literature, it is concluded that the existing 1D gas side resistance models have reasonable accuracy with less complexity

compared to multi-dimensional and gas-solid side resistance models. As a result, a 1-D GSR numerical model is adopted in this thesis, a detailed explanation of the theoretical model can be found in Chapter 2.

1.4.2. Heat and mass transfer in developing boundary layer region

The motion of a fluid that creates velocity, temperature, and concentration gradients, must comply with several laws of nature namely, conservation of energy, momentum and chemical species as well as Newton's 2nd law of motion [49].

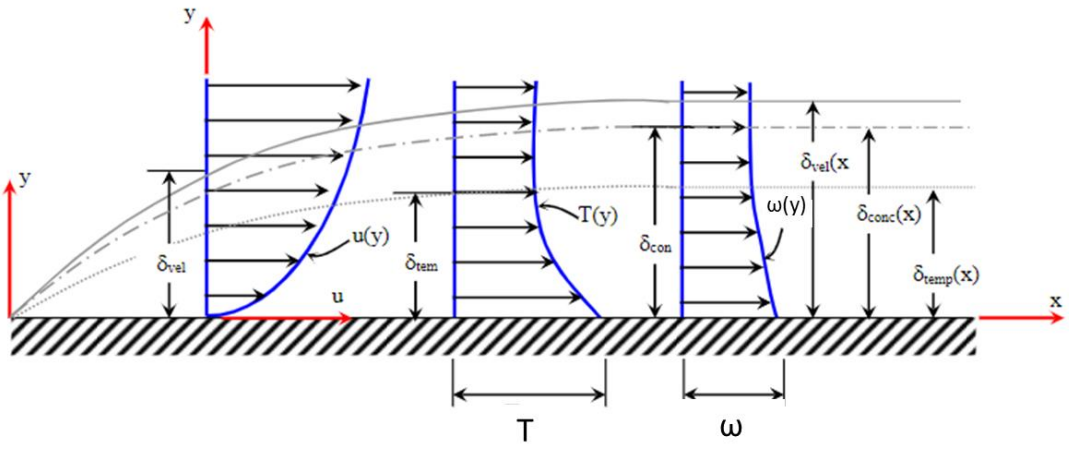

Figure 9 Velocity (u), temperature (T) and concentration (ω) profiles and related boundary layers shown for flow over a flat plate

In the vicinity of the wall, where viscous forces dominate over inertial forces, a hydrodynamic boundary layer region develops. As the fluid moves along the surface,see Figure 9, the boundary layer thickness (δ_{vel}) increases until it reaches to fully developed region in which the velocity profile does not change anymore. With the similar concept, temperature and concentration profiles reach to fully developed region as the thermal and concentration boundary layers (δ_{temp}, δ_{conc}) grow. These three boundary layers are related to the surface friction, convective heat transfer and convective mass transfer rates; are analogous. Therefore when the convective mass transfer coefficient (h_m) can be calculated if the convective heat transfer (h) coefficient is known as given in Eq. (7), where Lewis number (Le) is the ratio of thermal diffusivity to mass diffusivity and n is a positive exponent that is commonly assumed as 1/3 [49].

$$\frac{h}{h_m} = c_p Le^{1-n} \tag{7}$$

Conventionally rotary desiccant wheels are fabricated in the form of honeycomb or sinusoidal shape mini channels e.g. 10^{-6} m^{-6} cross sectional area and relatively large length e.g. 0.1 - 0.5 m. The entrance length (developing boundary layer region) is negligible for such geometry therefore, it is a common assumption to consider fully developed flow for modelling the desiccant wheel channels [29], [44]. However, for the proposed sorbent disc geometry, the flow is interrupted by the spacing between multiple discs. In the entrance region the convective heat and mass transfer coefficients are higher compared to fully developed region as the surface temperature or concentration are much different than the mean temperature or concentration of the flow [49]. Therefore, an analytical model as explained in detail in Chapter 2.1.2, is required to calculate the convective heat transfer coefficient (h) in the developing region and use the heat and mass transfer analogy to relate the convective mass ttransfer coefficient (h_m).

Chapter 2. Theoretical modeling

2.1. Heat and mass transfer model

Side view of an air channel surrounded with sorbent wall is shown in Figure 10. Air side and sorbent side control volumes are connected by heat and mass transfer through the air/sorbent interface. In the present model, the conservation of energy and concentration of water vapor equations should be solved to predict the transient temperature and moisture concentration of air and sorbent layer throughout the channel. During the inhale period, the air stream at the inlet of the channel, return air (RA), is dehumidified as it flows through the channel. It leaves the channel as exhaust air (EA) with less water vapor content. During the exhale period, dry outdoor air (OA) enters the channel at the opposite inlet of the channel, recovers the water vapor stored in the sorbent wall in previous inhale period. Cycle time-averaged temperature and moisture concentration of air at the outlet of the channel, indicates the EA and SA conditions of the sorbent bed, respectively.

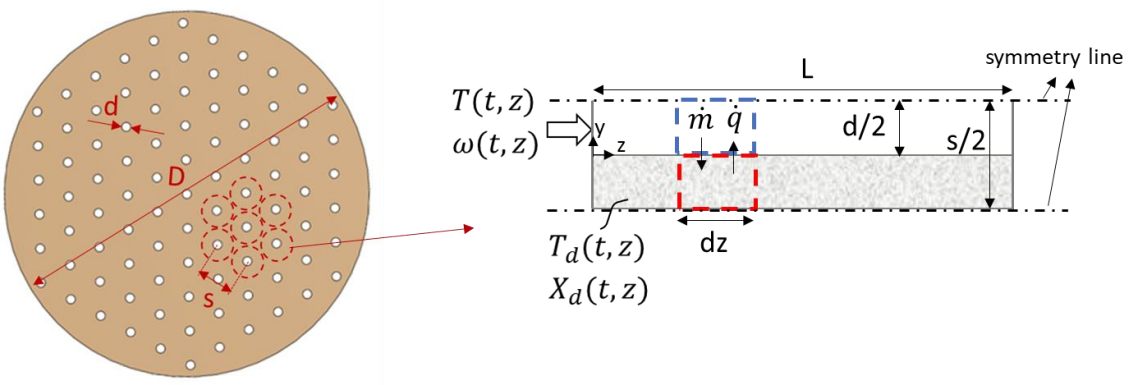

Figure 10 Air side and sorbent side control volumes are shown on a unit channel of the sorbent disc

Main assumptions for the present 1D gas side resistance model are listed below:

1. All air channels on the discs are identical, therefore heat and mass transfer in a unit channel is modeled as a representative of the entire disc, see Figure 10. The outlet air conditions are considered as the inlet air conditions for the successive disc.

2. Laminar flow is assumed for the channel because the Reynolds number is typically less than 2300. Both for modeling and experimental study, air velocity in the unit channels are between 1.5 to 3 m/s ensuring laminar flow assumption.

3. The heat and mass transfer in the unit channel is modeled using bulk mean temperatures and moisture concentrations of the air (mean bulk temperature and moisture concentration are assumed for air flow within each discrete dz unit)[34], [50]

4. Thermal boundary layer and concentration boundary layer develop simultaneously as the Lewis number is approximately one [34], [51]. This assumption is used to relate the convective mass transfer coefficient (h_m) to convective heat transfer coefficient (h).

5. The axial heat conduction and mass diffusion are neglected (z-direction) in both air and sorbent control volumes [5].

6. Thermo-physical properties of dry air and dry sorbent are assumed to be constant with respect to temperature, bulk properties are calculated as a function of moisture content.

2.1.1. Governing equations

Energy and mass conservation equations are solved for air and sorbent wall simultaneously. Figure 11 schematically shows the mass balance in air and sorbent control volumes. In air control volume, the net moisture increase rate is equal to the sum of the net moisture influx by air flow and moisture transfer through the sorbent interface as given in Eq. (8) :

$$\rho_a A_{cs} \frac{\partial \omega_a}{\partial t} + u \rho_a A_{cs} \frac{\partial \omega_a}{\partial z} + h_m P \left(\omega_a - \omega_d \right) = 0 \qquad (8)$$

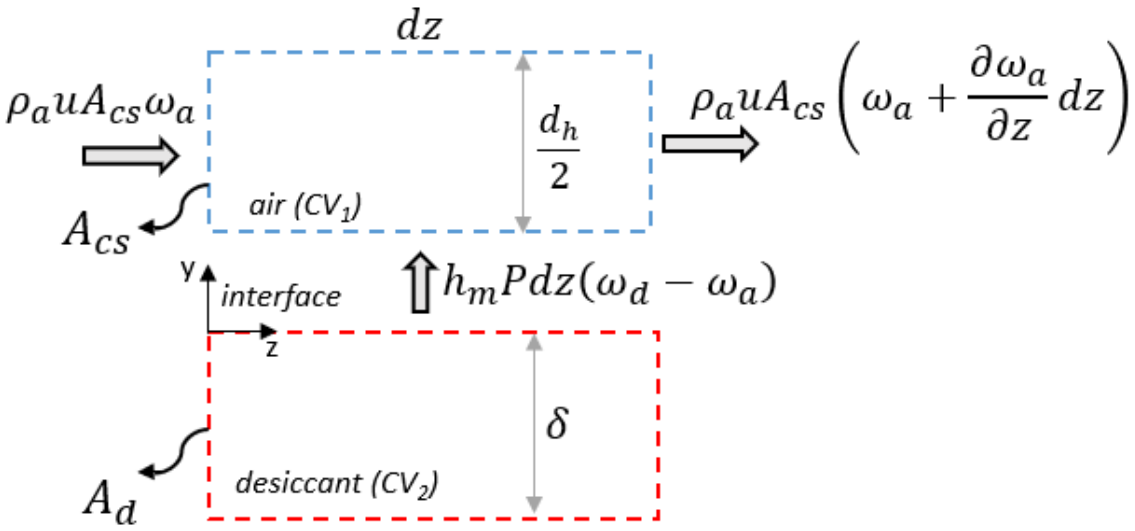

Figure 11 Mass balance in air and sorbent control volumes

In the sorbent control volume, the rate of moisture increase in the sorbent material and the pores is equal to the mass transfer through the interface. In Eq. (9) the first term refers to the rate of moisture change in the sorbent pores in vapor form and the second term refers to the water in sorbent material in adsorbed form. ε is pore volume, ω_d (g/g air) is specific humidity in the pore volume in gas form and X_d (g/g_d) is the water uptake in the sorbent material.

$$A_d dz \left[\rho_a \varepsilon \frac{\partial \omega_d}{\partial t} + \rho_d (1-\varepsilon) \frac{\partial X_d}{\partial t} \right] + h_m P dz (\omega_d - \omega_a) = 0 \qquad (9)$$

In the sorbent layer, there is an equilibrium relation between the adsorbed water and the water vapor existing inside the pores in vapor form. This relation is expressed by isotherms which are obtained experimentally and have various shapes and slope depending on the sorbent material type. Water sorption isotherm of the silica gel $CaCl_2$ composite is measured using a thermogravimetric analyzer (IGA-002, Hiden Isochema), available in our laboratory. A 4th order polynomial was fitted to the isotherm data to express a correlation between vapor partial pressure (RH_d) with water uptake (X_d):

$$RH_d = 0.0078 - 0.05759 X_d + 24.16554 X_d^2 - 124.478 X_d^3 + 204.226 X_d^4 \qquad (10)$$

By means of psychometric relations, vapor partial pressure (RH_d) in the sorbent can be used to calculate humidity ratio in the sorbent (ω_d):

$$\omega_d = \frac{0.62188 RH_d}{\left(\frac{P}{P_{vs}} - RH_d\right)} \tag{11}$$

where saturation pressure is a function of sorbent temperature:

$$P_{vs} = e^{(23.196 - 3816.44/(T_d - 46.13))} \tag{12}$$

Energy balance in the air stream and sorbent control volumes are shown in Figure 12. Rate of energy storage in the air control volume is related to the convective heat transfer through the sorbent interface and enthalpy of the air stream in and out of CV.

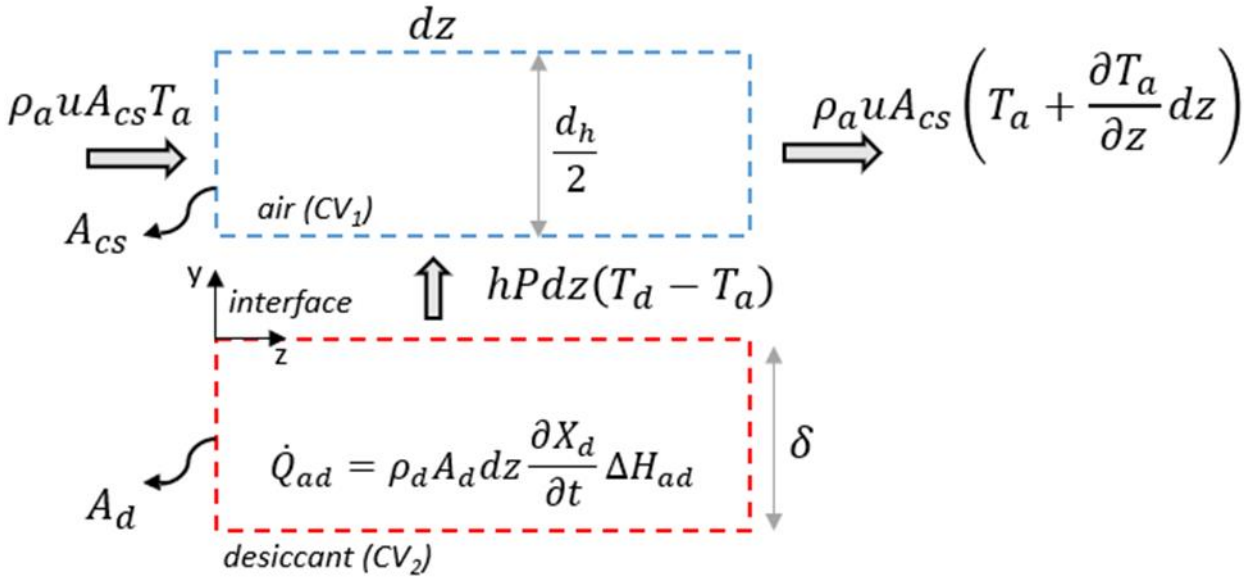

Figure 12 Energy balance in air and sorbent control volumes

Accordingly, an energy balance in the air control volume is written as Eq. (13):

$$\rho_a c_{p,a} A_{cs} \frac{\partial T_a}{\partial t} + u \rho_a c_{p,a} A_{cs} \frac{\partial T_a}{\partial z} + hP\left(T_a - T_d\right) = 0 \tag{13}$$

In the sorbent layer, there is an additional source term to account for heat source/sink due to heat of adsorption.

$$\rho_d c_{p,d} A_d \frac{\partial T_d}{\partial t} - hP\left(T_a - T_d\right) - \rho_{d,dry} A_d \frac{\partial X_d}{\partial t} \Delta H_{ads} = 0 \tag{14}$$

Here in Eq. (14) it is assumed that the heat of adsorption is generated inside the sorbent layer and written in sorbent energy balance equation as a source/sink term, following previous studies on desiccant wheel (DW) modeling [34], [37], [41], [52]–[55].

Heat of adsorption is a property depending on sorbent type and uptake. For silica gel, it is very close to the latent heat of evaporation of water and it can be taken as a constant, 3,378 kJ/kg [56]. However, there is an available correlation to calculate the heat of adsorption based on instantaneous uptake, which is used in this study for silica gel RD [57]:

$$\Delta H_{ads} = \begin{cases} -12400 X_d + 3500 & X_d \le 0.05 \\ -1400 X_d + 2900 & X_d > 0.05 \end{cases} \tag{15}$$

2.1.2. Heat and mass transfer coefficients

In enthalpy exchangers, air velocity in the channels is usually between 1.5 to 3 m/s corresponding to Reynolds number less than 300. Therefore, the air flow regime inside the air channels is laminar. Fluid flow and heat and mass transfer problems in non-circular ducts are usually solved by non-dimensionalization of the equations by hydraulic diameter (d_h):

$$d_h = \frac{4A}{P} \tag{16}$$

where A is the channel face area, and P is the wetted perimeter of the channel. Although hydraulic diameter is conventionally used in literature, it causes issues due to the mismatch between the area computed by the hydraulic diameter and the actual area of the channel. Square root of the channel's cross-sectional area, given in Eq. (17), is shown

to be a more suitable characteristic length by a non-dimensional analysis performed on arbitrarily shaped channels and validated by analytical, numerical, experimental data from the literature [58].

$$L_{ch} = \sqrt{A} \tag{17}$$

Analytical solutions for laminar fully developed flow [59] and thermally developing flow [60] were presented for arbitrary cross sections using square root of area as the characteristic length. Entrance length for hydrodynamic boundary layer (L_h) and thermal boundary layer (L_t) are defined as below [61], [62]:

$$L_h = 0.0822 \in (1+\in)^2 \left[1 - \frac{192 \in}{\pi^5} \tanh\left(\frac{\pi}{2 \in}\right)\right]^2 \tag{18}$$

$$L_t = 19.80 \left(\frac{C_2 C_3}{C_1}\right)^3 \in^{1+3\gamma} (1+\in)^2 \left[1 - \frac{192 \in}{\pi^5} \tanh\left(\frac{\pi}{2 \in}\right)\right]^2 \tag{19}$$

where $\in$ is the aspect ratio of the duct, C_1, C_2, C_3 are constant parameters determined by boundary conditions (uniform heat flux or uniform temperature) and γ is the shape parameter. γ, defines the upper and lower bounds for different channel shapes i.e. rectangular is in the upper bound and triangular in the lower bound.

Table 3 Coefficients based on boundary conditions and channel shape [60]

Boundary Conditions		
UWT	C_3=0.409, C_1=3.24	$f(Pr) = \frac{0.564}{[1+(1.664Pr^{1/6})^{9/2}]^{2/9}}$
UWF	C_3=0.501, C_1=3.86	$f(Pr) = \frac{0.886}{[1+(1.664Pr^{1/6})^{9/2}]^{2/9}}$
Nusselt number type		
Local	C_2=1	C_4=1
Average	C_2=3/2	C_4=2
Shape parameter		
Upper bound	$\gamma = 1/10$	
Lower bound	$\gamma = -3/10$	

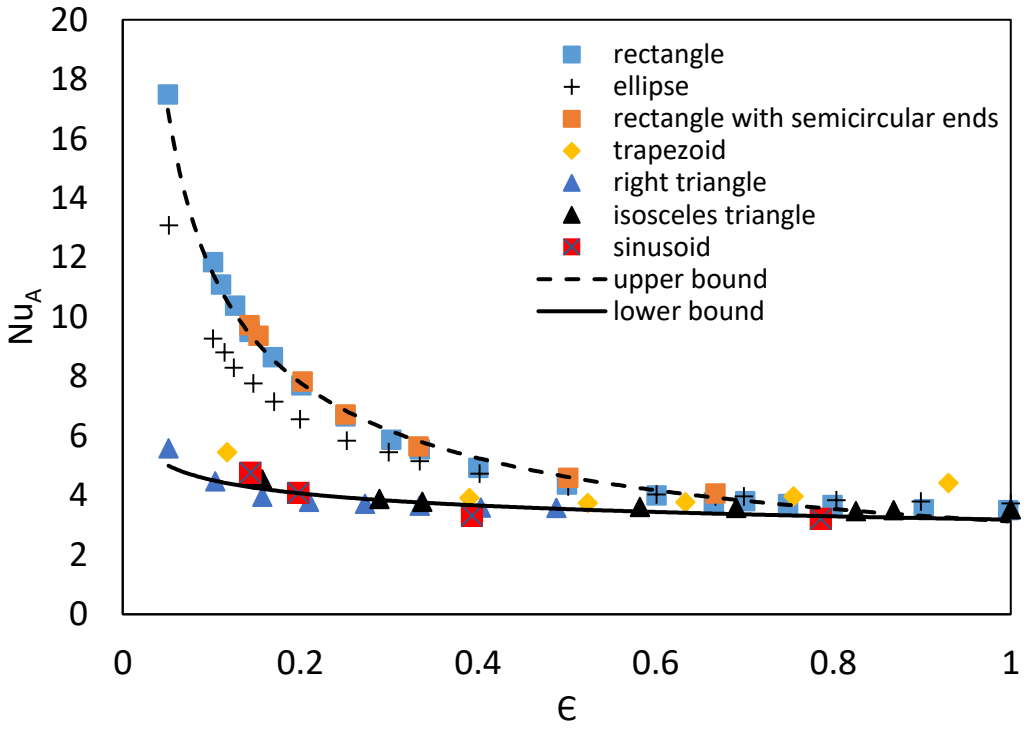

Figure 13 Nusselt number for various cross-section geometries versus aspect ratio [60], [63], [64]

Muzychka and Yovanovich [58], [60] developed an analytical model that accurately predicts Nusselt number (Nu) for combined entrance region by combining the asymptotic

results for laminar boundary layer flow and Graetz flow for the thermal entrance region. Using the square root of the channel's cross-sectional area as the characteristic length, solutions for similar geometries collapsed onto a single curve as seen in Figure 13. Shape parameter γ, defines the upper and lower bounds for different channel shapes i.e. rectangular is in the upper bound and triangular in the lower bound. Sadeghi et al. [63] proposed an algorithm to evaluate the similarity of the channel shapes and predict the Nu based on polar moment of inertia of different geometries. Friction coefficients and Nusselt numbers are calculated for fully developed and developing flow regimes by following correlations based on geometry of the channels [60].

Fully developed flow friction coefficient:

$$f\,\mathrm{Re} = \frac{12}{\sqrt{\in}\left(1+\in\right)\left[1-\frac{192\in}{\pi^5}\tanh\left(\frac{\pi}{2\in}\right)\right]} \tag{20}$$

Nusselt number:

$$Nu = C_1\left(\frac{f\,\mathrm{Re}}{8\sqrt{\pi}\,\in^{\gamma}}\right) \tag{21}$$

Developing flow friction coefficient:

$$f\,\mathrm{Re}_d = \left[\left(\frac{12}{\sqrt{\in}\left(1+\in\right)\left[1-\frac{192\in}{\pi^5}\tanh\left(\frac{\pi}{2\in}\right)\right]}\right)^2 + \left(\frac{3.44}{\sqrt{z^+}}\right)^2\right]^{1/2} \tag{22}$$

Local Nusselt number:

$$Nu\left(z^*\right) = \left[\left(\frac{C_4 f(\mathrm{Pr})}{\sqrt{z^*}}\right)^m + \left(\left\{C_2C_3\left(\frac{f\,\mathrm{Re}}{z^*}\right)^{1/3}\right\}^5 + \left\{C_1\left(\frac{f\,\mathrm{Re}}{8\sqrt{\pi}\,\in^{\gamma}}\right)\right\}^5\right)^{m/5}\right]^{1/m} \tag{23}$$

Average Nusselt number in the developing flow region:

$$\overline{Nu} = \frac{\int_0^{L_{ch}} Nu\left(z^*\right) dz^*}{L_{ch}} \tag{24}$$

In the air channel surrounded with sorbent wall neither heat flux nor the temperature of the sorbent wall is constant. Therefore, an averaged Nusselt number used to calculate the convective heat transfer coefficient for either fully developed or developing flow regimes.

$$Nu = \frac{Nu_T + Nu_H}{2} \tag{25}$$

$$h = k_a Nu / d_h \tag{26}$$

Similarities between energy, momentum and diffusion equations are commonly used to obtain velocity, temperature and concentration profiles. Reynolds analogy can be used to relate velocity and temperature profiles if Prandtl number is close to 1. Similarly, Chilton-Colburn analogy suggests that temperature and concentration profiles can be related by Lewis number given in Eq. (27) and Eq.(28) below.

$$Le = \frac{\alpha}{D} \tag{27}$$

$$h_m = \frac{h}{\rho_a c_{p,a} Le^{2/3}} \tag{28}$$

Lewis number is the ratio of thermal diffusion to mass diffusion to compare the temperature and concentration boundary layer thicknesses. For air, Lewis number can be assumed to be one, which leads to identical (non-dimensionalized) thermal and concentration boundary layers.

Pressure drop through the channel is calculated from friction factor and entrance/ exit losses [65].

$$\Delta P = \frac{\rho_{air} u_{air}^2}{2}\left(\frac{4f\,\mathrm{Re}\,L}{\sqrt{A}} + f_{entrance/exit}\right) \tag{29}$$

2.1.3. Initial and boundary conditions

At both ends of the sorbent channel, insulated and impermeable boundaries are assumed [34], [54]:

$$\frac{\partial T_a}{\partial z} = \frac{\partial \omega_a}{\partial t} = 0, \quad \text{at } x = 0, L \tag{30}$$

Periodic return (RA) and outdoor (OA) air conditions are applied inlet conditions with reversed flow direction for n number of cycles.

$$\begin{aligned} T_a &= T_{RA} \qquad \text{at } t = 0 + nt_{cycle} \\ \omega_a &= \omega_{RA} \end{aligned} \tag{31}$$

$$\begin{aligned} T_a &= T_{BU} \quad \text{at t} = t_{exhaust} + nt_{cycle} \\ \omega_a &= \omega_{OA} \end{aligned} \tag{32}$$

2.1.4. Solution procedure and verification

Coupled energy and mass balance equations are discretized along the disc thickness using a finite element method. Mathematical equations are written and solved in Matlab 2018a. Four partial differential equations (energy and mass balance equations) along with the desiccant isotherm equation are solved for five variables (T_a, T_d, ω, ω_d, X_d) using 4th order Runge-Kutta iteration method.

Table 4 Test conditions for preliminary test

	Condition 1	Condition 2	Condition 3
Cycle time (s)	600	1200	1200
Air flow rate (CFM)	9.8	6.3	4.4
Return air temperature, T_{RA} (°C)	21	22	22
Return air specific humidity, ω_{RA} (g_w/kg_a)	4.9	4.5	4.6
Outdoor air temperature, T_{OA} (°C)	22	24	24
Return air specific humidity, ω_{OA} (g_w/kg_a)	0.6	0.9	0.8

The model is verified with preliminary experimental data collected at three different operating conditions as listed in Table 4. Testbed description and details of the experimental study is reported in Chapter 3. Comparison of the model and experimental data in terms of VCOP and ε_L are shown in Figure 14. The model and experimental data are in good agreement within a 6.5% difference. Further verification of the model the experimental data at several different operating conditions can be found in Chapter 4.1 of this thesis.

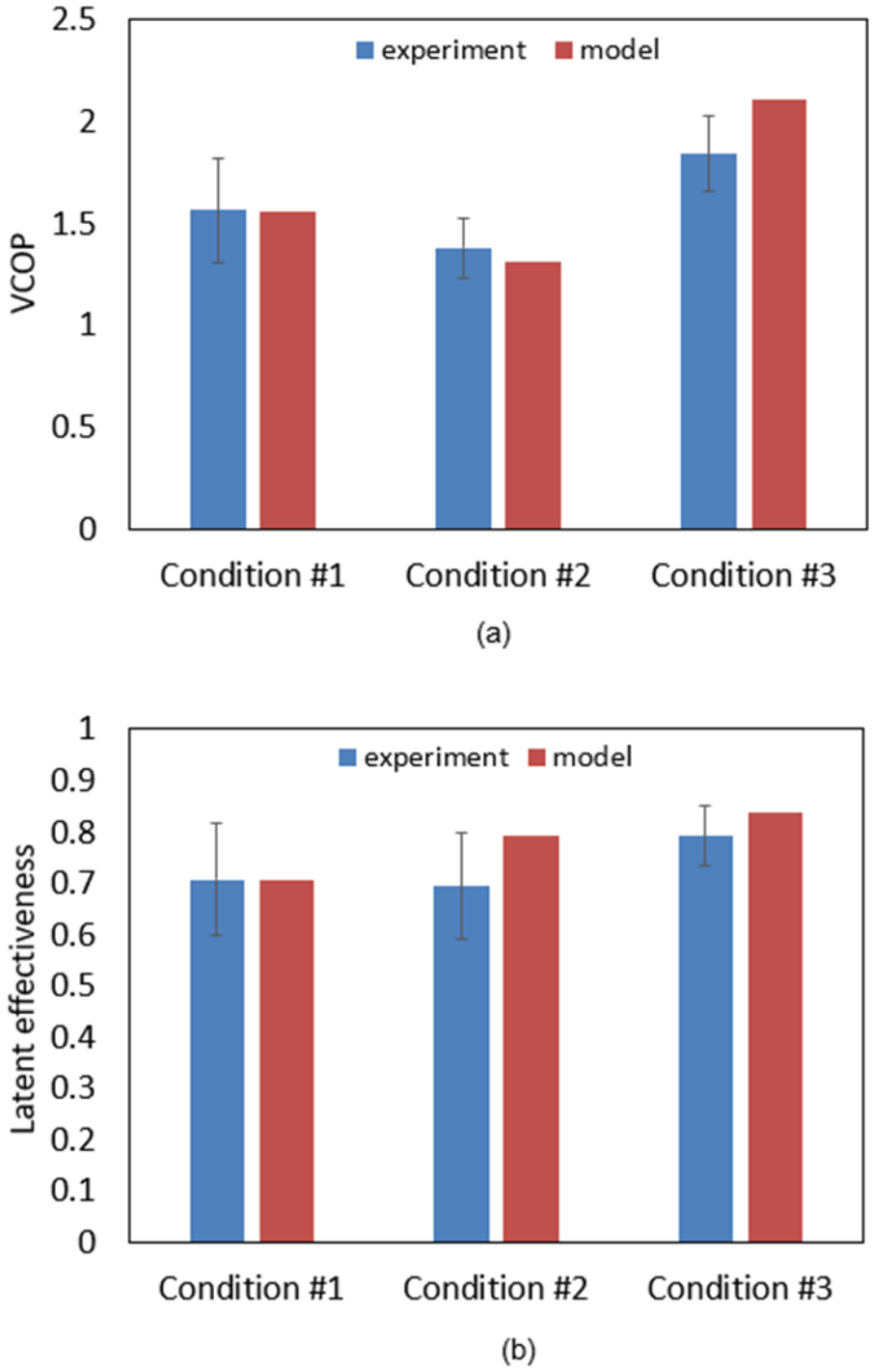

Figure 14 Verification of model with experimental data a) VCOP, b) latent effectiveness

2.1.5. Sensitivity analysis to design a proof of concept sorbent discs unit

In order to build a proof of concept sorbent discs unit to test at laboratory conditions, a preliminary sensitivity analysis is conducted using the theoretical model. The diameter of the disc is chosen as a constant design parameter, 8", considering the size of the experimental set-up built in our laboratory and the available size of molds to build the discs. The HRV/ERV units are sized by a design face velocity, or air velocity in the channels, which is between 1.5 to 3 m/s for conventional applications [29]. The proof of concept sorbent disc is designed based on an air velocity of 2.5 m/s per channel. The effect of air flow rate, air face velocity in other words, on SERV performance is studied both numerically and experimentally in Chapter 4 of this thesis.

Constant design parameters for the sensitivity analysis are listed in Table 5. The diameter and number of air channels, as well as the number of sorbent discs, are studied for the proof of concept design.

Table 5 Constant design parameters for sensitivity analysis

Disc diameter (D)	203.2 mm (8")
Disc thickness (L)	27 mm
Return air temperature (T_{RA})	22°C
Return air specific humidity (ω_{RA})	8.6 g_w/kg_a
Outdoor air temperature (T_{OA})	-10°C
Outdoor air specific humidity (ω_{OA})	1 g_w/kg_a
Between units temperature (T_{BU})	13°C
Half cycle time ($t_{halfcycle}$)	60 s
Air velocity in the channel (u_a)	2.5 m/s

Effect of the channel diameter to the spacing ratio (d/s) and number of the channels

The performance of sorbent discs with air channel diameter varying from 2.5 mm to 20 mm is studied. The disc diameter, sorbent mass, sorbent wall thickness around the channels and air velocity per channel are equal for all the studied designs. The number of channels is the largest for smaller channel diameter design as shown in Figure 15. As the channel diameter (d) increases, spacing (s) between the channels increases; the total air-sorbent surface area decreases. The channel diameter to the spacing ratio (d/s) is an important design parameter that compares both the volume of air with the volume of sorbent and the air -sorbent surface area (A_s).

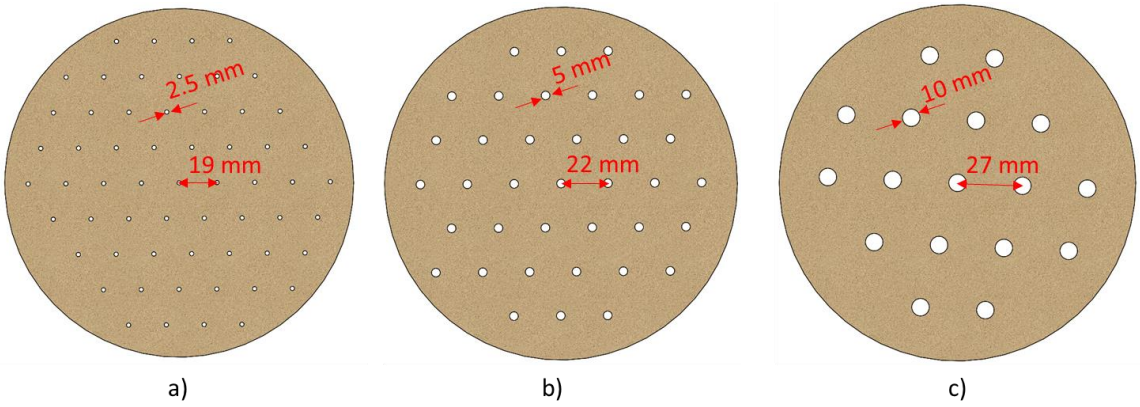

Figure 15 Variation of channel diameter a) d=2.5 mm, s=19 mm, A_s = 2.1 cm^2, b) d=5 mm, s=22 mm A_s = 1.1 cm^2, c) d=10 mm, s=27 mm, A_s = 0.3 cm^2

Effect of channel diameter to space ratio (d/s), in the range of 0.08 - 0.35, is investigated in terms of ε_L, VCOP and MRC* and shown in Figure 16, Figure 17, and Figure 18. The total air -sorbent surface area (A_s) in the channels, is the largest for the design with smallest and highest number of channels, 3.5 cm^2. A_s decreases as the channels size increase and the number of channels decrease; the smallest A_s for this study is 0.25 cm^2 for the 20 mm diameter channel design.

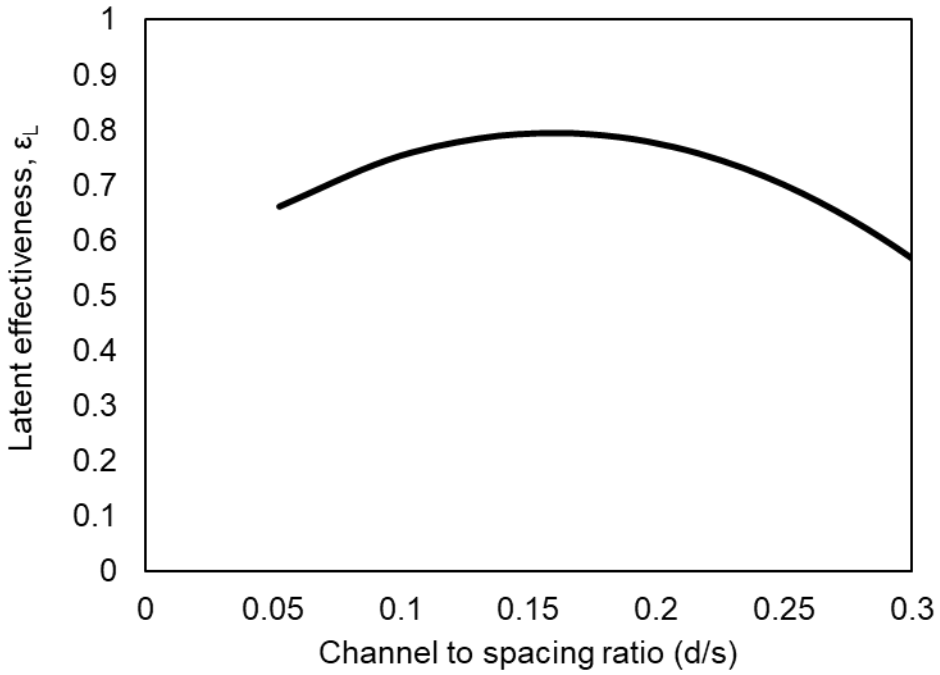

Figure 16 Latent effectiveness for channel diameter 1.5 mm to 20 mm (or diameter to space ratio (0.8 to 0.3)

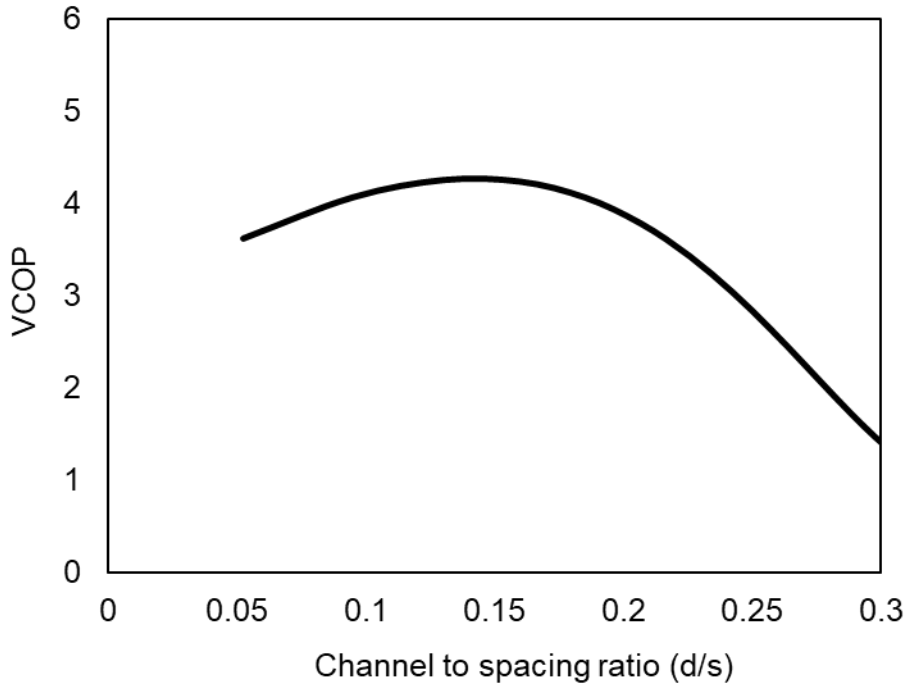

Figure 17 VCOP for channel diameter 1.5 mm to 20 mm (or diameter to space ratio (0.8 to 0.3)

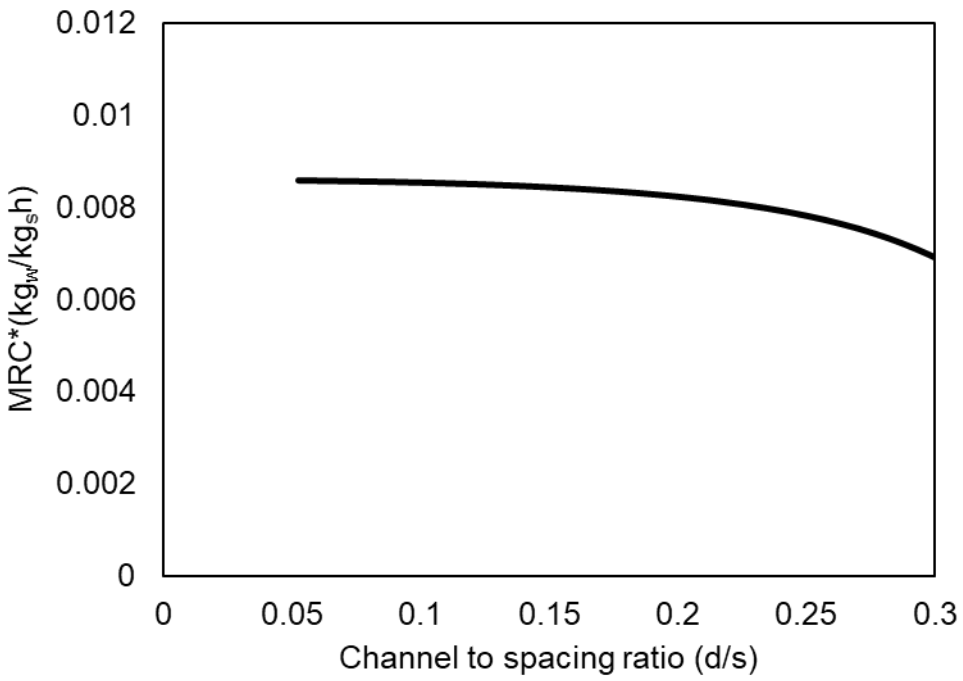

Figure 18 MRC* for channel diameter 1.5 mm to 20 mm (diameter to space ratio (0.8 to 0.3)

It is shown in Figure 16, that ε_L decreases as the d/s increases, that is expected due to the decrease in the air – sorbent surface area (A_s). MRC* has the same trend as the total mass of sorbent is equal in all studied designs. As indicated by ε_L and MRC* a sorbent disc design with smaller and higher number of channels has higher moisture recovery capacity. However small air channels cause higher pressure drop. The effect of pressure drop is included in VCOP calculation as fan power. As expected, VCOP has a maximum point that indicates optimum moisture recovery that is achieved with optimum fan power.

Effect of number of discs

Due to limitations of the manufacturing method, for this study the disc thickness (L), is considered 27 mm for all the designs. The overall thickness of the sorbent discs unit is determined by number of the sorbent discs. The spacing between the discs assumed to be large enough to ensure boundary layer interruption which is experimentally tested and validated in Chapter 4.

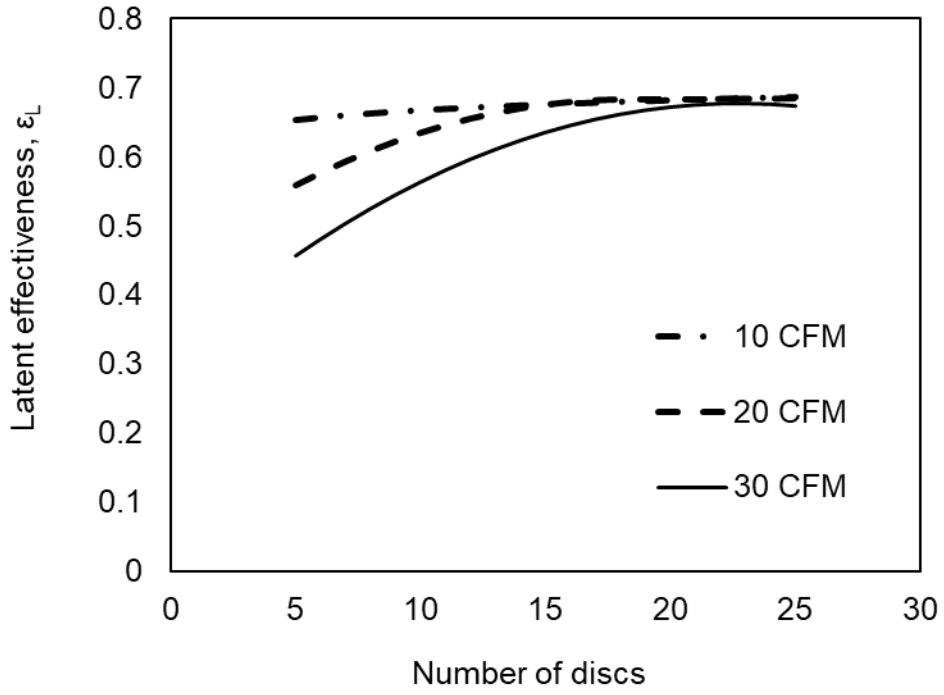

Figure 19 Effect of number of discs on latent effectiveness at 10, 20 and 30 CFM air flow rates

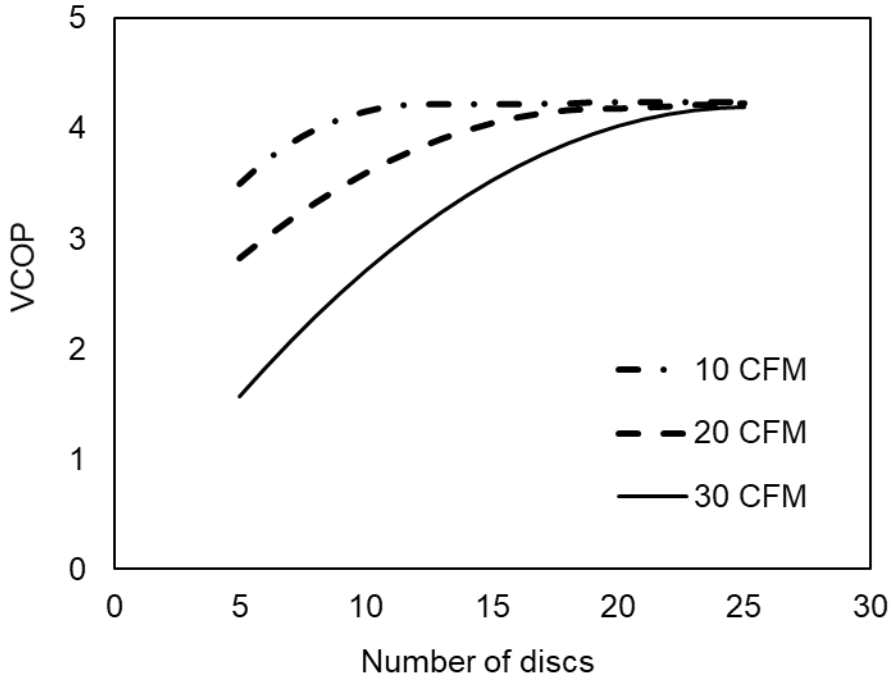

Figure 20 Effect of number of discs on VCOP for 10, 20 and 30 CFM air flow rates

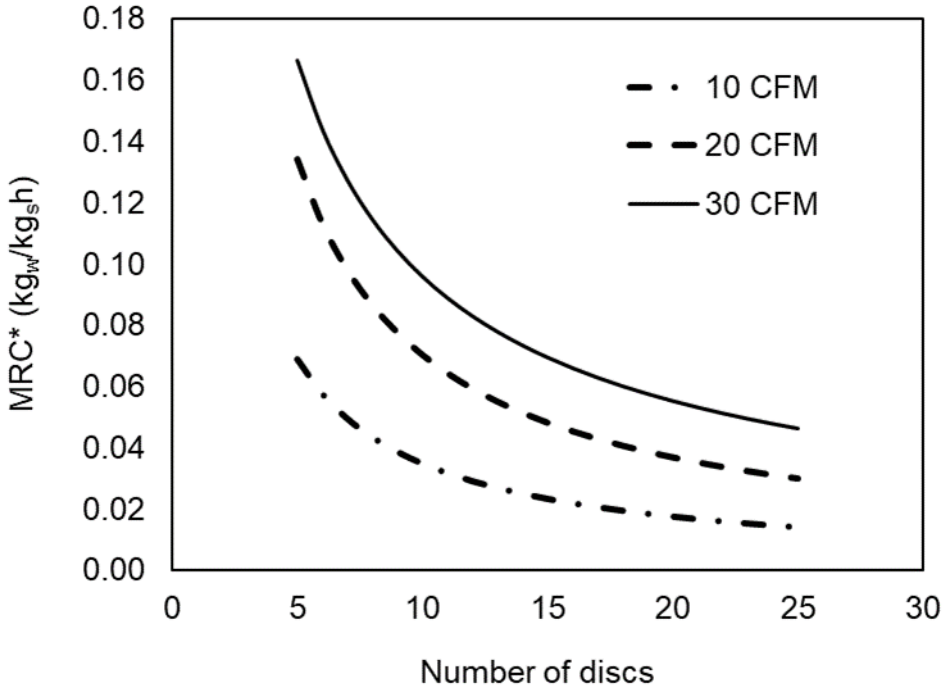

Figure 21 Effect of number of discs on MRC* for 10, 20 and 30 CFM air flow rates

Increase in the number of discs from 5 to 25 discs is investigated for three different air flow rates, 10, 20, 30 CFM. ε_L, VCOP and MRC* are plotted in Figure 19, Figure 20, Figure 21. At lower flow rate, 10 CFM, increasing the number of discs does not improve the ε_L significantly. At higher flow rates, the sorbent discs are in contact with a higher amount of moisture, therefore, there is a higher potential for moisture uptake. The ε_L decreases at higher air flow rates. However, as the number of discs increases, the ε_L reaches to a maximum value as shown in Figure 19.

Increase in the flow rate and number of discs, also increase the pressure drop, therefore, the change in VCOP is more significant compared to ε_L, see Figure 20. As opposed to the increase in water uptake of larger number of discs; the mass of the sorbent increases significantly; result in a decrease in the MRC*.

Conclusions of the sensitivity analysis

Preliminary analysis on channel diameter, number of channels and number of discs, provide the design features for the proof of concept sorbent discs that are tested in the experimental set-up built in our laboratory. The laboratory scale experimental set-up is designed to test the performance of SERV up to 20 CFM. Considering the preliminary analysis on the theoretical model, 8" diameter sorbent discs with 69 air channels of 5 mm diameter (d/s = 0.2) is built, see Chapter 3. For the sorbent discs unit built with 5 discs the ε_L and VCOP drops about 15% as the air flow rate increases from 10 to 20 CFM. When the number of discs increases the ε_L and VCOP at different flow rates approach to the maximum; however the increase in the total mass of the sorbent results in a decrease in MRC^*. Therefore, a 15% decrease in ε_L and VCOP is found tolerable and 5 sorbent discs are built for the laboratory scale tests.

Details of the experimental set-up and a brief description of the preparation procedure of sorbent discs with the design parameters are presented in Chapter 3 of this thesis.

Chapter 3. Experimental study

3.1. Sorbent disc sample preparation

Sorbent material selection for the moisture recovery bed is an essential step to design an effective and compact sorbent-based enthalpy recovery ventilator (SERV). To achieve better moisture recovery performance, the sorbent bed should feature high uptake capacity and uptake rate, high heat of sorption and low pressure drop. Previously Aristov et al. [66] experimentally studied the performance of different sorbent materials and different pellet size. They tested commercially available sorbents alumina oxide (Al_2O_3), KSM silica gel and custom-made alumina oxide modified with 10-12% $CaCl_2$ (IK-011-1) at cyclic sorption (humid)/ regeneration (dry) conditions with 5 to 31 m^3/h air flow rate. They concluded that IK-011-1 outperforms the commercially available sorbents by 1.3 to 1.8 times higher moisture uptake. They also compared two different pellet sizes for IK-011-1 sorbent and showed that the efficiency of moisture removal increased with a decrease in the pellet size. The smaller size IK-011-1 (1.8 mm diameter, 6 mm length pellets) was chosen as the best sorbent, however causing the highest pressure drop.

In the present study, silica gel (SiliaFlash® B150, Silicycle Inc.,Quebec, Canada) which has high surface area due to small pellet size (0.25 to 0.5 mm in diameter according to the supplier) was selected. To further increase the uptake capacity, it is impregnated with $CaCl_2$. This consolidated sorbent should be bind together to prevent moving away with the air flow during operation. After a number of trials on the amount of binder; composition of 55%wt silica gel B150, 30%wt $CaCl_2$ and 15%wt Polyvinylpyrrolidone (PVP40) binder (40,000 MW, Sigma-Aldrich) was found to be mechanically stable to be placed in the SERV.

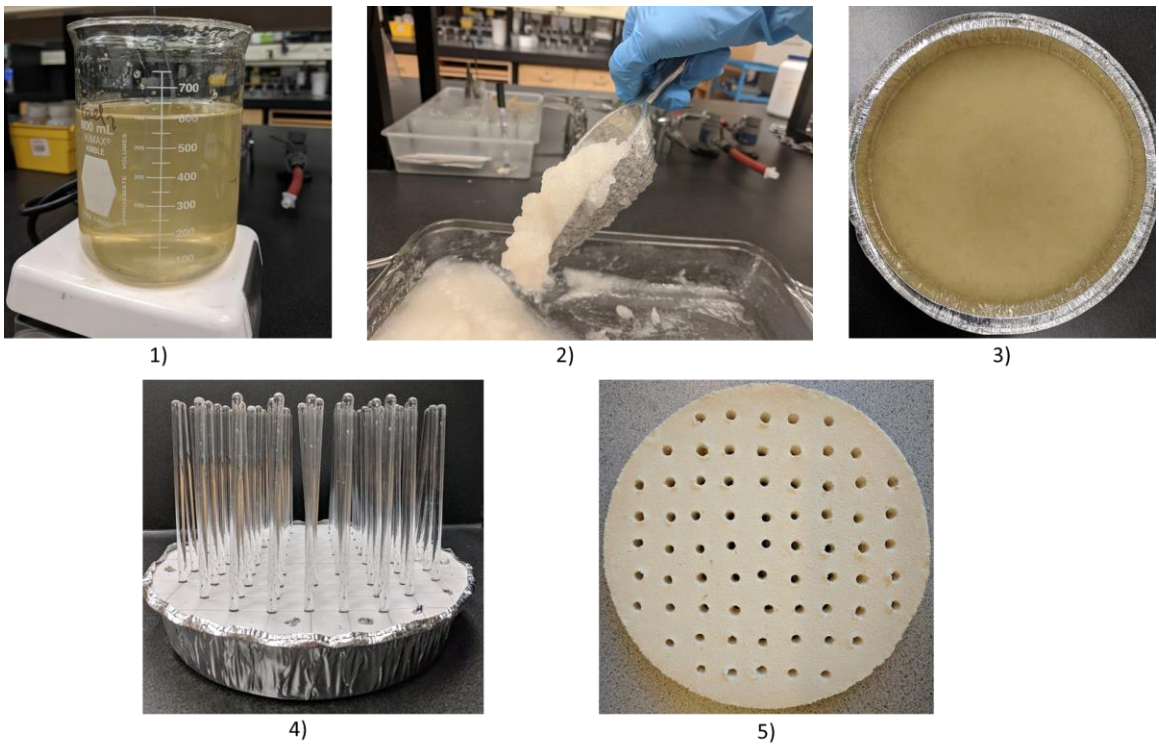

Figure 22 Sample preparation steps

Composite sorbent discs were prepared in the following steps as shown in Figure 22:

1. 150 g $CaCl_2$ and 75 g PVP40 binder were solved in 500 ml water and mixed with a magnetic stir bar until a homogeneous binder solution was achieved

2. A slurry composite was obtained by mixing the binder solution with 270 g silica gel B150

3. The mixture was poured in an 8” diameter aluminum baking container

4. 69 glass rods with 5 mm diameter each, were inserted through the aluminum cover which is formed to create equal distance (2 cm spacing) between the channels. Vents created on the cover to help vapor removal while drying

5. The mixture was dried in an oven gradually by 80-120-150°C temperature steps for 1.5-3-3 hours. Glass rods and the cover were removed at the last 2 hours. The composite sorbent disc was removed from the aluminum container. Residuals in the air channels were cleaned using the glass rods.

Following the same steps and using the same aluminum mold cover to forming the air channels, 5 composite sorbent discs each 516±15 g were prepared for the SERV heat and moisture recovery performance test.

3.2. Experimental set-up

A test bed as shown in Figure 23, has been built in our laboratory (LAEC) to measure the performance of the proposed SERV system. The test facility consisted of two environmental chambers, two fans, the test section, measurement devices and a data acquisition system (DAQ). An environmental chamber (Thermotron© Model XSE-3000-10-10) wass used to supply outdoor air down to -15°C, 80% RH up to 30 CFM. Indoor air condition at about 20-22°C and 35-50% RH, is prepared and supplied in the second environmental chamber (ESPEC© Model EPX-H2). Inhale and exhale air streams were supplied by intermittently operating two fans connected to each environmental chamber. Voltage regulators were connected to the fans to adjust the flow rates in each air stream. The air was driven to the environmental chamber, passed through the test section and reached to the environmental chamber at the other end. In the second half cycle, the flow was reversed by operating the second fan.

An orifice plate (4" Oripac© model 4150, beta: 0.5) mounted on a 4" duct with 34" straight length before and after (the duct section after the orifice plate was placed inside the environmental chamber due to spacing limitations) as per International Standard ISO 5167 [67], to measure the air flow rate by means of pressure differential.

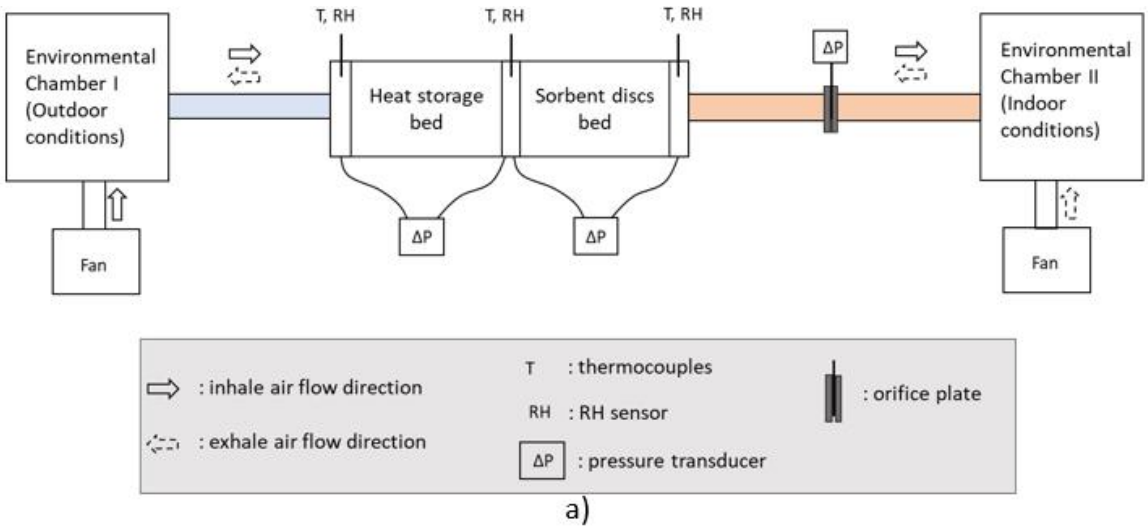

Figure 23 a) Schematic of the testbed showing the sensor locations, b) photo of the set -up built in our laboratory

The test section consists of a sensible heat storage bed and sorbent discs bed. The heat storage material (aquarium gravels, 2 kg) was placed in an 8” diameter circular duct. Five composite sorbent discs were built as described in section 3.1, and placed in an 8.5” diameter circular duct with 7.5 cm spacing in between each discs. The discs were surrounded by rubber window seal as shown in Figure 24.

Figure 24 Sorbent discs placed in an 8.5" duct with 7.5 cm spacing and sealed by a rubber seal

3.3. Test instruments and uncertainty analysis

To measure the performance of the proposed SERV, an experimental set-up was built in our laboratory based on ASHRAE standard 84 [15] as described in 3.2. Temperature and RH are measured before and after the heat storage bed and sorbent discs bed. The pressure differential was measured for both beds and the air flow rate was calculated using the pressure differential of the pressure taps on orifice plate as per International Standard ISO 5167 [67]. The model and accuracy of each instrument are listed in Table 6. Data collection was accomplished by a set of NI-SCXI data modules and chassis (National Instruments, Austin TX) connected to LabVIEW software installed on a computer. The thermocouples and RH sensors were calibrated and matched at several conditions in the test range, using the environmental chamber.

Uncertainty of each performance parameter (MRC^{*}, VCOP and latent/sensible effectiveness), were calculated considering error propagation as given in Eq.(33) [68].

$$s_f = \sqrt{\left(\frac{\partial f}{\partial x}\right)^2 s_x^2 + \left(\frac{\partial f}{\partial y}\right)^2 s_y^2 + \ldots} \quad \text{for } f(x,y,\ldots) \tag{33}$$

Table 6 Test instruments and uncertainties

Parameter	Instrument maker, model	Accuracy
RH	Vaisala HUMICAP® HMP110	± 1.5% for 0…+40°C ± 3.0% for -40 …0 °C
Temperature	Vaisala HUMICAP® HMP110	± 0.2°C for 0…+40°C ± 0.3°C for -40 …0 °C
	Omega, T type thermocouple	± 0.5 °C
Pressure difference	Setra Model 267, 0-5" W.C. low differential pressure transducer	± 1% of the full range
Orifice pressure difference	Setra Model 267, 0-0.5" W.C. very low differential pressure transducer	± 0.25% of the full range

As per ASHRAE standard 84 [15], the uncertainties related to sensible and latent effectiveness should be up to 5% and 7% relatively. However, there is no standard that applies for extreme cold climate conditions. Nasr et al. [69] experimentally studied the frost formation detection in membrane type ERVs, mentioned that at cold condition tests the high uncertainty (up to 12%) of latent effectiveness makes an unfavorable parameter for frost detection. High uncertainty in the extreme cold condition is mostly due to the RH measurement at the supply air inlet (sensor located at the cold and dry outdoor condition). In section 1.2, a novel performance parameter VCOP, is introduced. VCOP is less dependent on the humidity at the outdoor location compared to latent effectiveness, see Eq.(2) and Eq.(5). Smaller uncertainty of VCOP makes it a better parameter to rate the performance of ERVs as shown in performance analysis in Chapter 4.

3.4. Performance evaluation

Performance evaluation of commercial ERVs are described in ASHRAE Standard 84 [15]. Unlike the commercial ERVs, the SERV operates intermittently as equally timed sequential inhale and exhale periods as shown in Figure 25. Therefore, cyclic quasi-steady state approach is used to evaluate the performance, as opposed to steady-state conditions for conventional ERVs.

Each test was continued until the water vapor and energy imbalance between the inhale and exhale air streams was smaller than 0.2 as given in Eq. (34)-(35) per [15].

$$\frac{\left|\dot{m}_{OA}\omega_{OA} - \dot{m}_{SA}\omega_{SA} + \dot{m}_{RA}\omega_{RA} - \dot{m}_{EA}\omega_{EA}\right|}{\dot{m}_{\min}\left|\omega_{OA} - \omega_{RA}\right|} \tag{34}$$

$$\frac{\left|\dot{m}_{OA}h_{OA} - \dot{m}_{SA}h_{SA} + \dot{m}_{RA}h_{RA} - \dot{m}_{EA}h_{EA}\right|}{\dot{m}_{\min}\left|h_{OA} - h_{RA}\right|} \tag{35}$$

Once the energy and water vapor imbalances were satisfied, the performance parameters namely MRC^*, VCOP, ε_S and ε_L were calculated based on the average temperature, specific humidity and air flow rate. Performance parameters for the sample test shown in Figure 26 and Figure 27, calculated using Equations (1) presented in section 1.2 of this thesis and reported in Table 7.

Table 7 Performance parameters for the sample test

Air flow rate (CFM)	8.3 ± 0.1
Sensible effectiveness, ε_S	0.70 ± 0.02
Latent effectiveness, ε_L	0.73 ± 0.07
VCOP	2.65 ± 0.14
MRC^* (kg_w/kg_sh)	0.017 ± 0.001

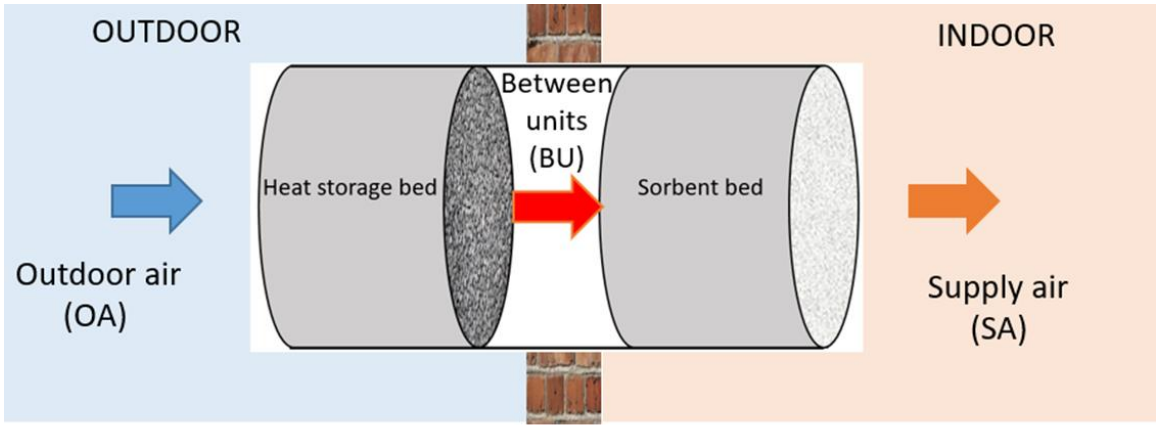

a) Inhale period

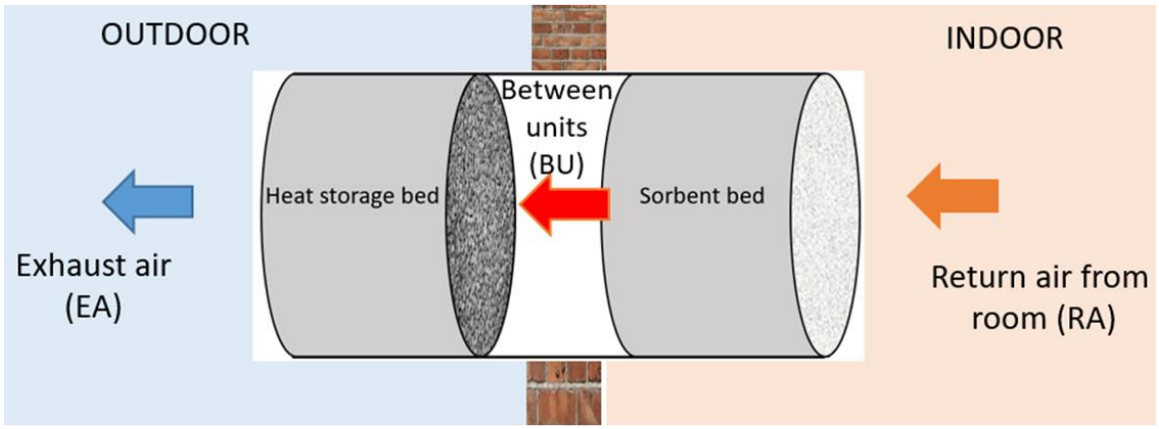

b) Exhale period

Figure 25 Air flow through the SERV unit during a) inhale, b) exhale periods

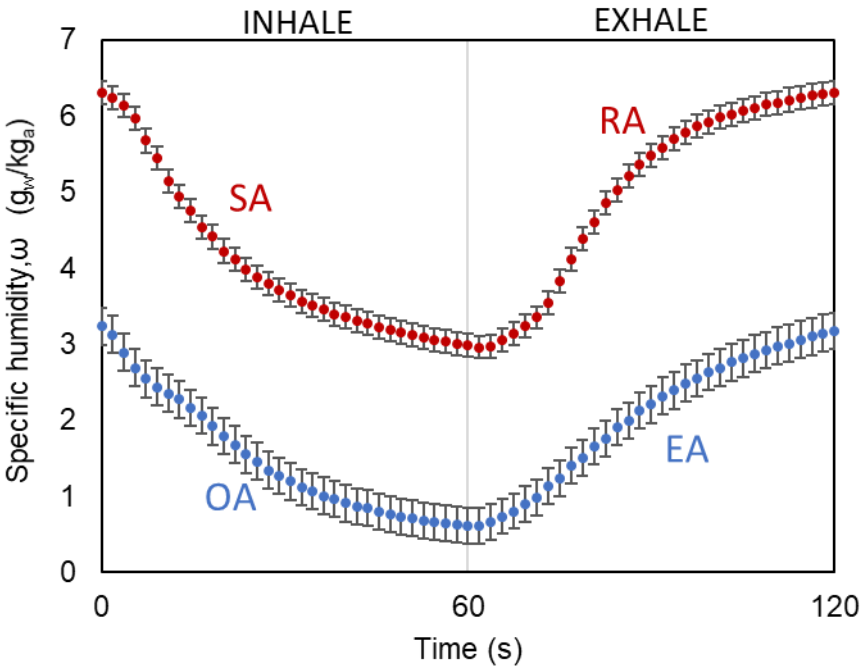

Figure 26 Specific humidity, ω, of outdoor air (OA) and supply air (SA) during inhale period; return air (RA) and exhaust air (EA) during exhale period

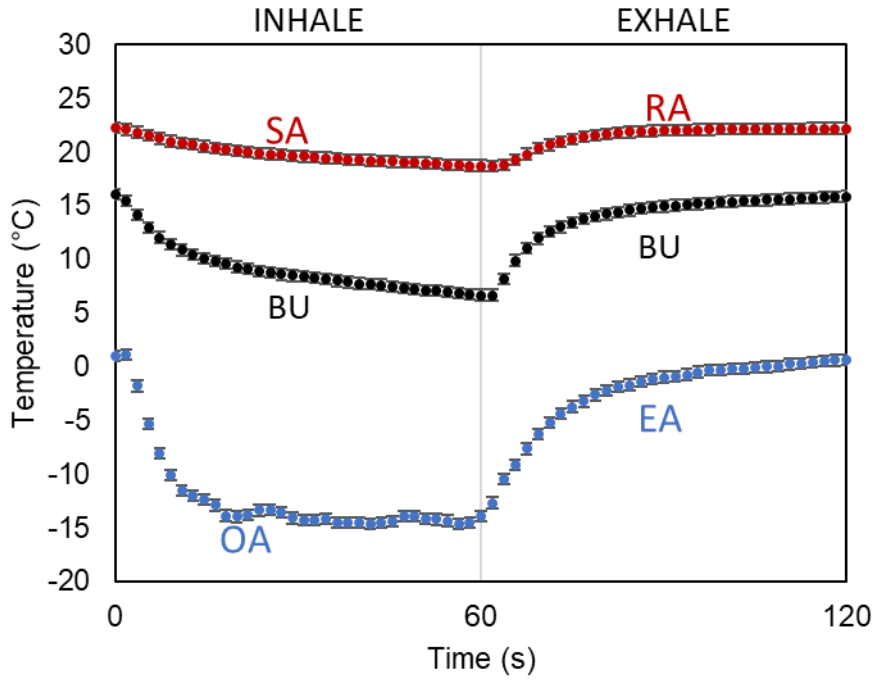

Figure 27 Temperature of outdoor air (OA) and supply air (SA) during inhale period; return air (RA) and exhaust air (EA) during exhale period

Sample temperature and specific humidity experimental data plots for exhale and inhale periods during the cyclic quasi-steady state are shown in Figure 26 and Figure 27. During the inhale period outdoor air (OA) with low specific humidity (0.5-3 g/kg), recovers the moisture in the sorbent bed, then flows to indoor as supply air (SA) with higher specific humidity (0.5-3 g/kg). In the following exhale period, the sorbent disc bed captures the humidity from the humid return air (RA) and releases it to the outdoor as dry exhaust air. Similarly, the heat storage bed comprised of 2.5 kg gravels recover 103 W of heat, increasing the temperature of the outdoor air (OA) from about -15°C to 7°C in average at the location between units (BU).

Chapter 4. Performance analysis

4.1. Operational conditions parametric study

4.1.1. Effect of air flow rate

The flow rate of the air, passing through the sorbent bed is one of the most critical parameters that affect the performance of SERV. Similar to membrane or desiccant wheel type ERVs, SERV should be sized based on the minimum required air flow rate. For the sorbent geometry described in Chapter 3, a set of experiments were performed at similar air inlet conditions and with air flow rate varying from 6 to 17 CFM listed in Table 8. The theoretical model, presented in Chapter 2, was run for air flow rates from 0 to 20 CFM. Laminar flow assumption of the model would not be valid for flow rates higher than 20 CFM for the mentioned sorbent disc geometry. Therefore, maximum flow rate, 20 CFM is chosen to keep the air flow in the laminar flow regime to be able to compare with the theoretical model as well as mechanical strength concerns of the sorbent discs.

Table 8 Operational conditions for the experimental data

	Test 1	Test 2	Test 3	Test 4	Test 5	Test 6
Air flow rate (CFM)	3.3 ±0.1	6.1±0.1	8.2±0.1	10.4±0.1	12.7±0.1	16.9±0.1
Cycle time (s)	60	60	60	60	60	60
Indoor temperature (°C)	22.6±0.5	22.1±0.5	21.9±0.5	20.6±0.5	20.2±0.5	20.6±0.5
Indoor specific humidity (g_w/kg_a)	5.0	4.6	5.0	4.2	4.7	5.1
Mid unit temperature (°C)	17.3±0.5	14.0±0.5	11.7±0.5	8.5±0.5	6.8±0.5	6.3±0.5
Outdoor temperature (°C)	0.3±0.5	9.4±0.5	-3.7±0.5	-6.3±0.5	-5.2±0.5	-7.6±0.5
Outdoor specific humidity (g_w/kg_a)	1.2	1.4	1.7	1.4	1.4	1.6

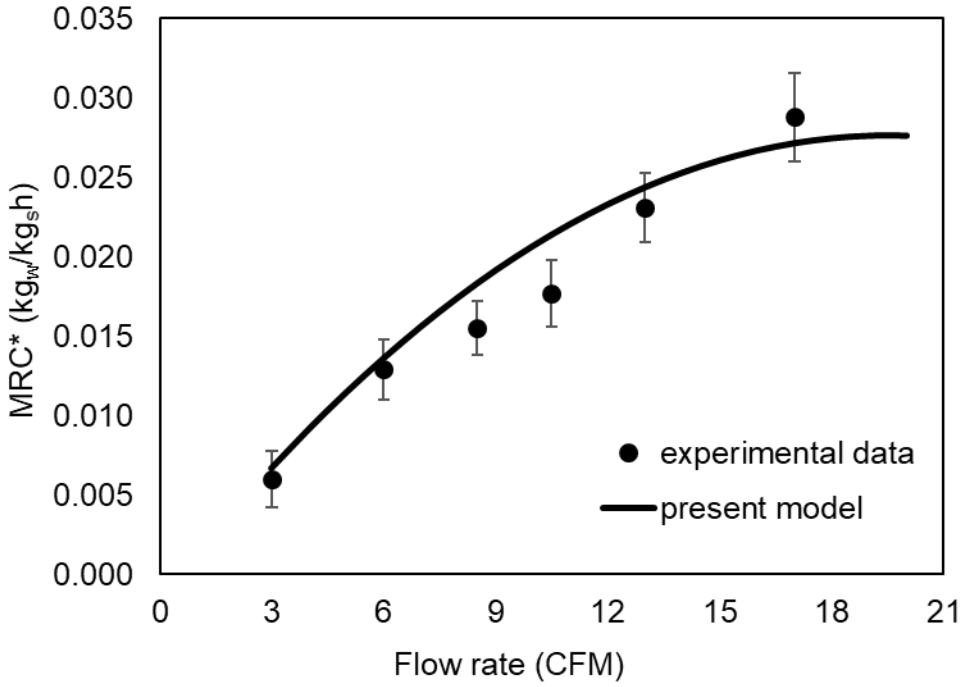

Figure 28 MRC* for various air flow rates compared against the present model, Chapter 2

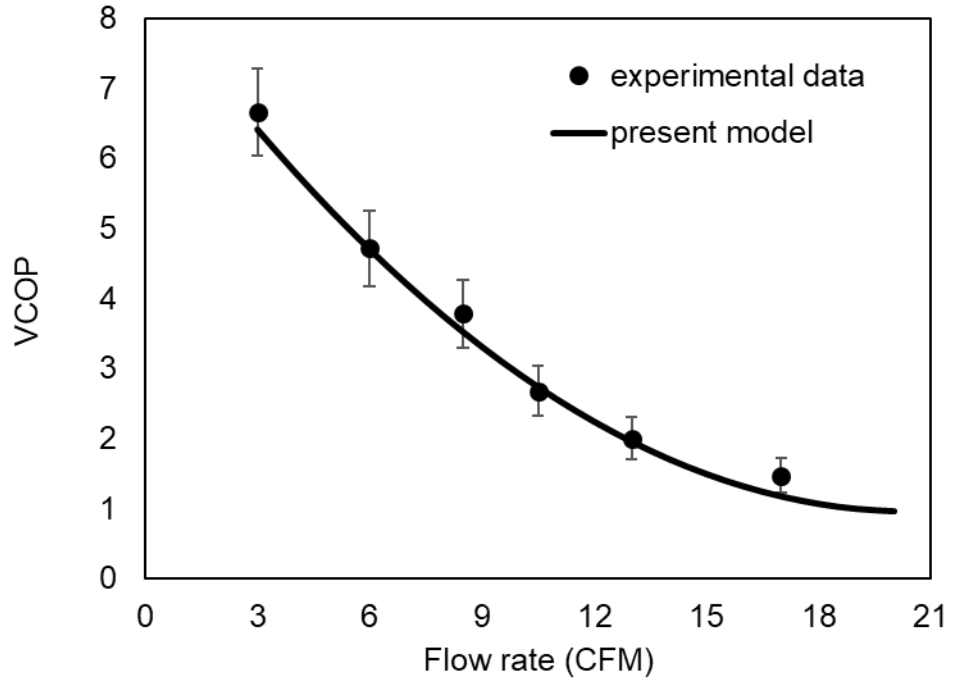

Figure 29 VCOP for various air flow rates compared against the present model, Chapter 2

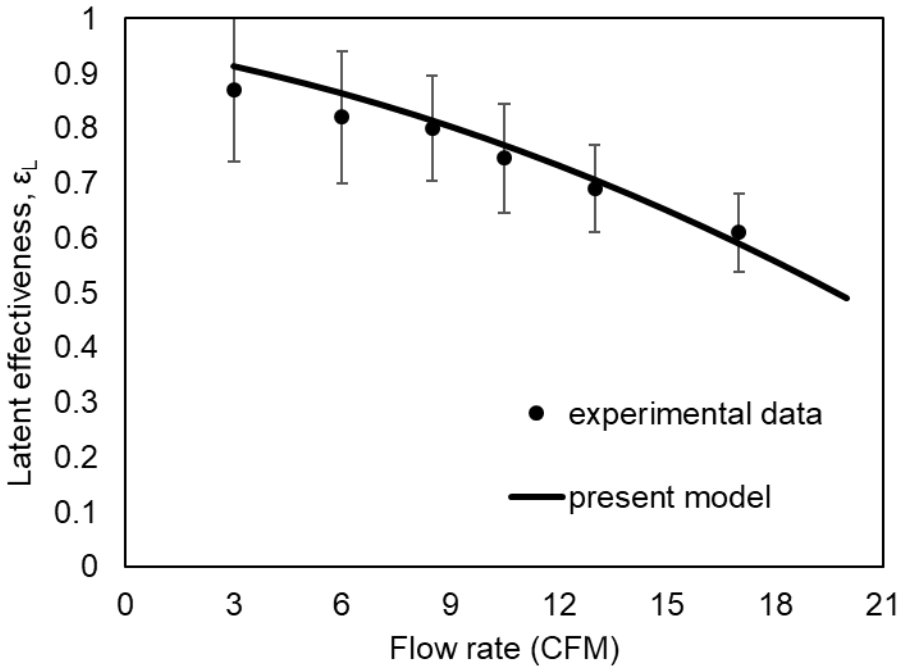

Figure 30 Latent effectiveness for various air flow rate compared against the present model, Chapter 2

Performance of SERV in terms of ε_L, VCOP and MRC^* for air flow rates varying up to 20 CFM is shown in Figure 28, Figure 29 and Figure 30. As expected, at higher flow rates the amount of water vapor that could be captured from the air is higher. Therefore, the sorbent discs can capture more water vapor resulting in an increase in MRC^*. However, the increase in water uptake is less than the increase in the total amount of water vapor in the air at higher flow rates. Therefore, both latent effectiveness and VCOP have a decreasing trend.

In commercial buildings, the minimum air flow rate required per person is approximately 15 CFM based on the International Mechanical Code® (IMC, 2015) [70] which is an updated version of ASHRAE 62.1 [5]. The proof of concept SERV can provide the required fresh air per person. The analysis of increasing flow rate shows that increasing the air velocity decreases the effectiveness. For larger scale applications, the system should be scaled up by increasing the disc diameter in order to keep the face velocity and pressure drop constant.

4.1.2. Effect of cycle time

SERV is an intermittently operated device and operates sequentially, equally timed inhale and exhale periods. Effect of half cycle time ranging from 30 s to 300 s is studied. In all tests, the indoor air conditions were about 21-22 °C, 27-32% RH, 4.6-5.5 g_w/kg_a. The outdoor conditions were -4 to -8°C, 50 - 60% RH, 1.1 - 1.4 g_w/kg_a.

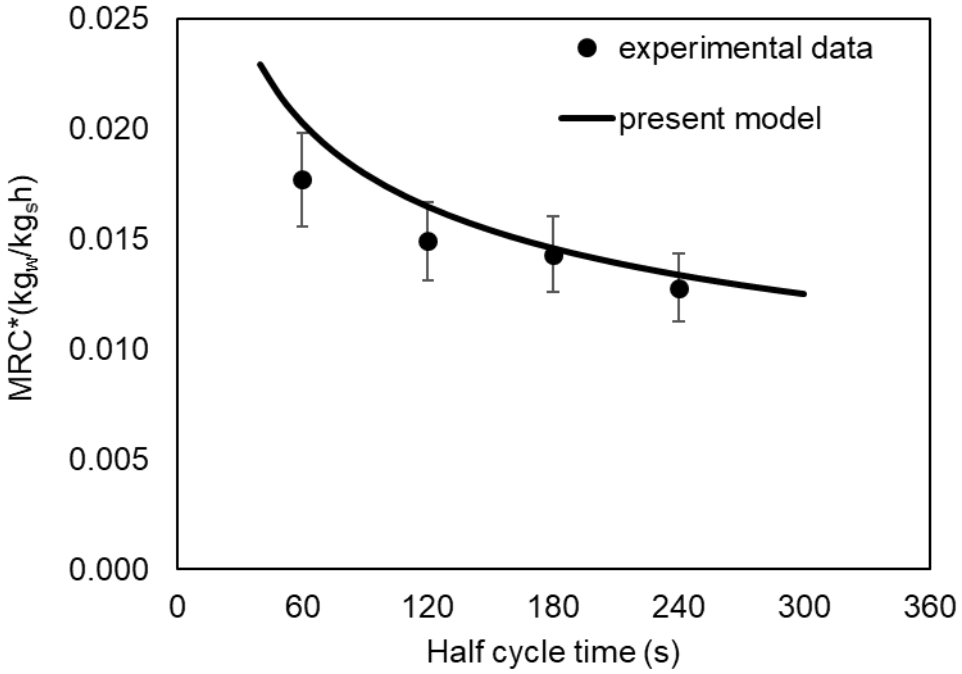

Figure 31 MRC* for various half cycle times (equally timed inhale and exhale) compared against the present model, Chapter 2

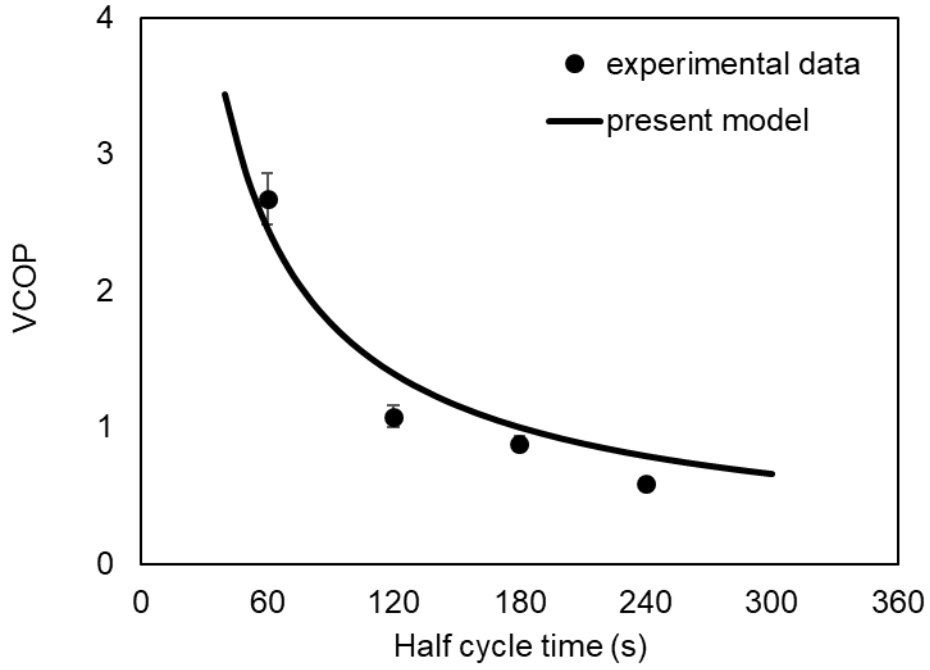

Figure 32 VCOP for various half cycle times (equally timed inhale and exhale) compared against the present model, Chapter 2

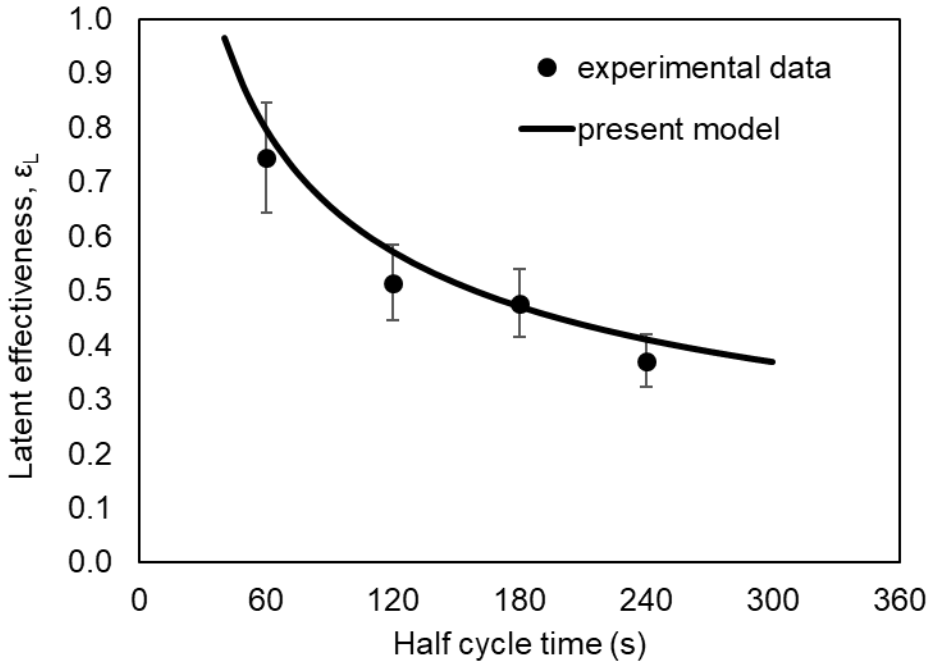

Figure 33 ε_L for various half cycle times (equally timed inhale and exhale) compared against the present model, Chapter 2

For all the studied flow rates the highest performance was achieved at a shorter cycle time. At the beginning of the inhale or exhale period, the vapor pressure difference between the air and sorbent is the highest. As the half cycle time increases the vapor pressure difference between the air and sorbent decreases that reduces the mass transfer rate. Therefore, a SERV operating with shorter cycle time has a higher mass transfer rate. As the cycle time increases MRC^* decrease and eventually reaches a plateau. The latent effectiveness and VCOP have similar decreasing trend with increasing cycle time.

4.1.3. Effect of outdoor air conditions

It is important to rate the performance of ERVs subjected to various climate conditions. As listed in Table 9, a set of experiments were performed at outdoor temperatures -21°C to 9.6°C. The capacity of the air to hold moisture decreases as the temperature decreases, therefore, the specific humidity ranges from 1.4 to 3.2 g_w/kg_a accordingly. The air flow rate was constant at about 8 CFM for all the tests.

Table 9 Operational conditions for climate variation tests

	Test 1	Test 2	Test 3	Test 4	Test 5
Air flow rate (CFM)	8.2±0.1	8.3±0.1	8.2±0.1	8.2±0.1	8.3±0.1
Cycle time (s)	60	60	60	60	60
Indoor temperature (°C)	21.3±0.5	21.3±0.5	21.9±0.5	22.0±0.5	22.3±0.5
Indoor specific humidity (g_w/kg_a)	5.0	5.0	5.0	5.1	5.2
Mid unit temperature (°C)	6.7±0.5	11.7±0.5	11.7±0.5	14.9±0.5	16.6±0.5
Outdoor temperature (°C)	-21.2±0.5	-12.0±0.5	-3.7±0.5	5.9±0.5	9.6±0.5
Outdoor specific humidity (g_w/kg_a)	1.4	1.4	1.9	2.4	3.2

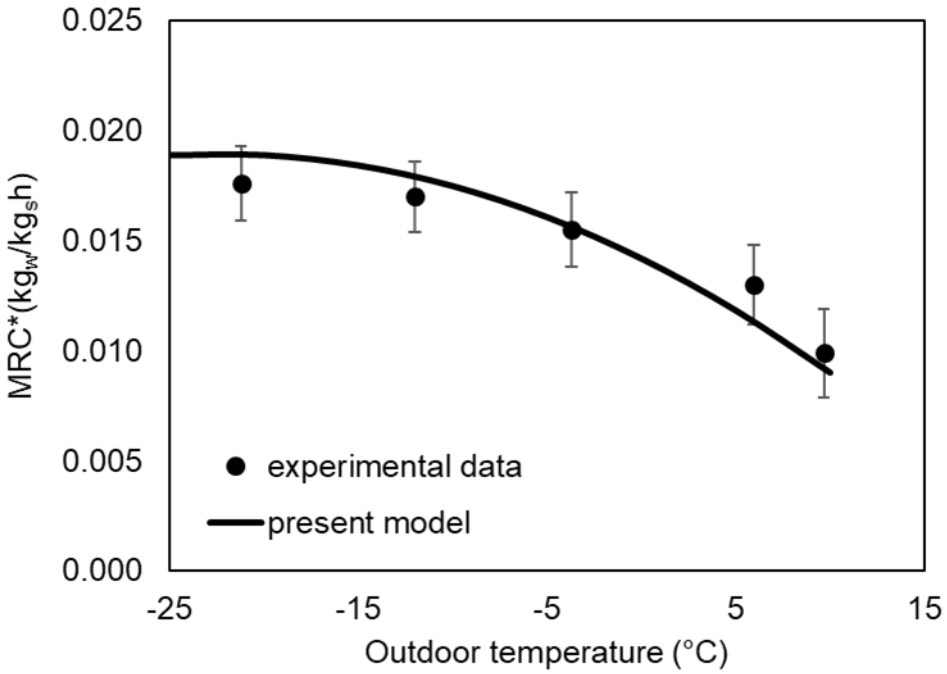

Figure 34 MRC* for various outdoor air conditions compared against the present model, Chapter 2

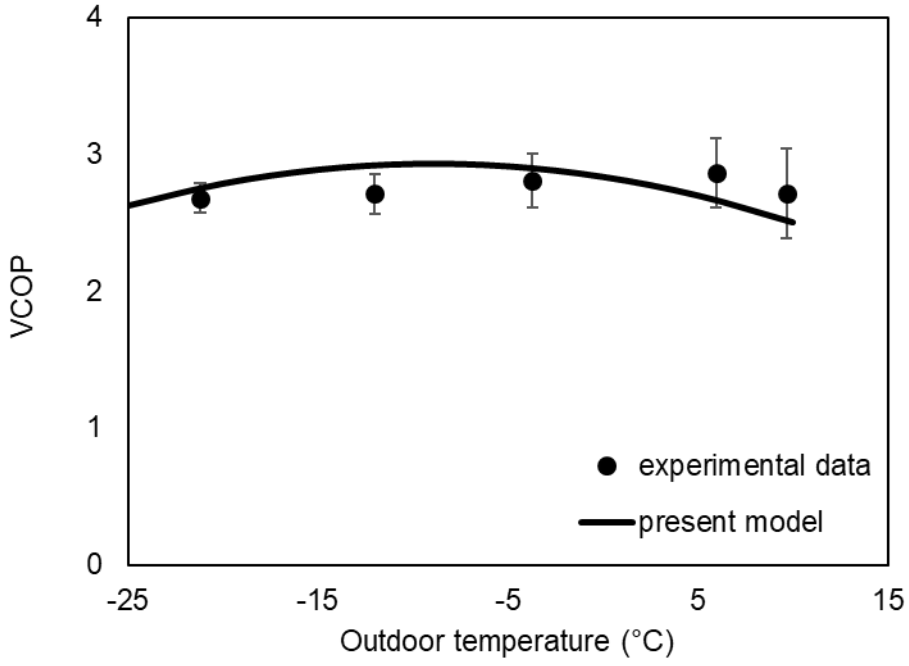

Figure 35 VCOP for various outdoor air conditions compared against the present model, Chapter 2

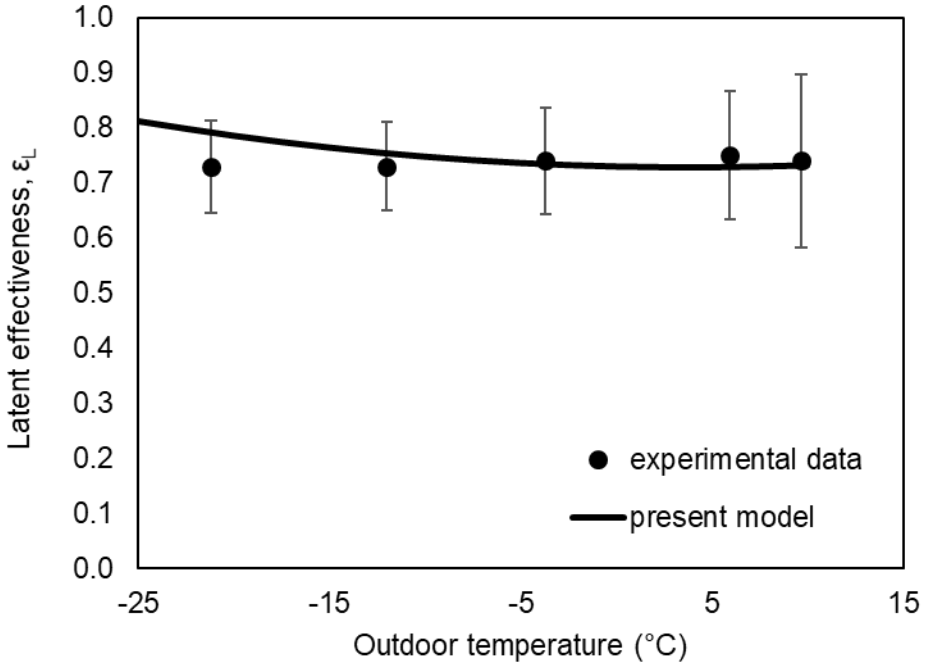

Figure 36 Latent effectiveness for various outdoor air conditions compared against the present model, Chapter 2

The performance of SERV at several winter outdoor conditions, -20°C to 10°C corresponding to specific humidity of 1.4 g_w/kg_a to 3.2 g_w/kg_a are shown in Figure 34, Figure 35, Figure 36. As shown in Figure 34, the MRC^* increases with a decrease in outdoor temperature. The specific humidity of the air decreases when the temperature decreases, therefore the humidity gap between indoor and outdoor enlarges, causing a higher need for humidity recovery. Therefore, the increase in the uptake does not affect latent effectiveness and VCOP significantly.

It is important to have a stable performance at several conditions for ERVs to operate throughout the season. The outdoor air condition variation analysis shows that SERV can operate at several different climates without significant deviation in the performance.

4.2. Performance comparison with packed bed sorption system

The proof of concept SERV system comprised of air channeled sorbent discs bed compared with a similar system based on a packed bed, called VENTIREG, made of alumina oxide impregnated with $CaCl_2$ ($Al_2O_3/CaCl_2$ (IK-011-1)) that was built and tested in Russia by Aristov et al. [66]. The packed bed of $Al_2O_3/CaCl_2$ (IK-011-1) with cylindrical pellets, 1.8 mm in diameter and 6 mm in length; ~3 kg in total was tested for air flow rates ranging from 3 to 18 CFM. The humid indoor air conditions were 20-22 °C, 27-30 %RH, dry outdoor air conditions were 17-20°C, 1.0-1.4 %RH. The specific humidity difference between indoor and outdoor air conditions was about 4.2-4.6 g_w/kg_a which is in the same range with the present experimental data collected from sorbent discs testbed as details listed in Table 10.

Table 10 Operational conditions of the sorbent discs experiments

	Test 1	Test 2	Test 3	Test 4	Test 5
Air flow rate (CFM)	6.1±0.1	8.3±0.1	10.5±0.1	14.3±0.1	16.1±0.1
Cycle time (s)	60	60	60	60	60
Indoor temperature (°C)	21.8±0.5	21.6±0.5	21.1±0.5	20.9±0.5	20.3±0.5
Indoor specific humidity (g_w/kg_a)	5.9	6.4	6.5	6.6	6.7
Mid unit temperature (°C)	15.9±0.5	13.2±0.5	10.7±0.5	8.5±0.5	8.1±0.5
Outdoor temperature (°C)	-21.2±0.5	-12.0±0.5	-3.7±0.5	5.9±0.5	9.6±0.5
Outdoor specific humidity (g_w/kg_a)	1.9	1.8	1.7	1.6	1.6
Specific humidity difference between indoor and outdoor (g_w/kg_a)	4.0	4.6	4.8	5.0	5.1

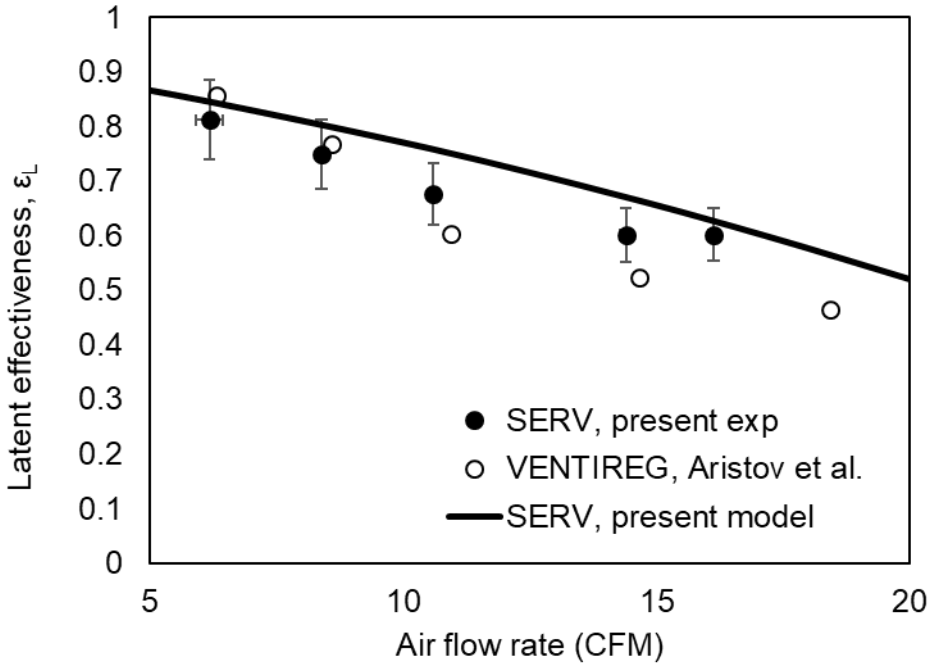

Figure 37 Comparison of latent effectiveness of sorbent discs (SERV) to packed bed system (VENTIREG)

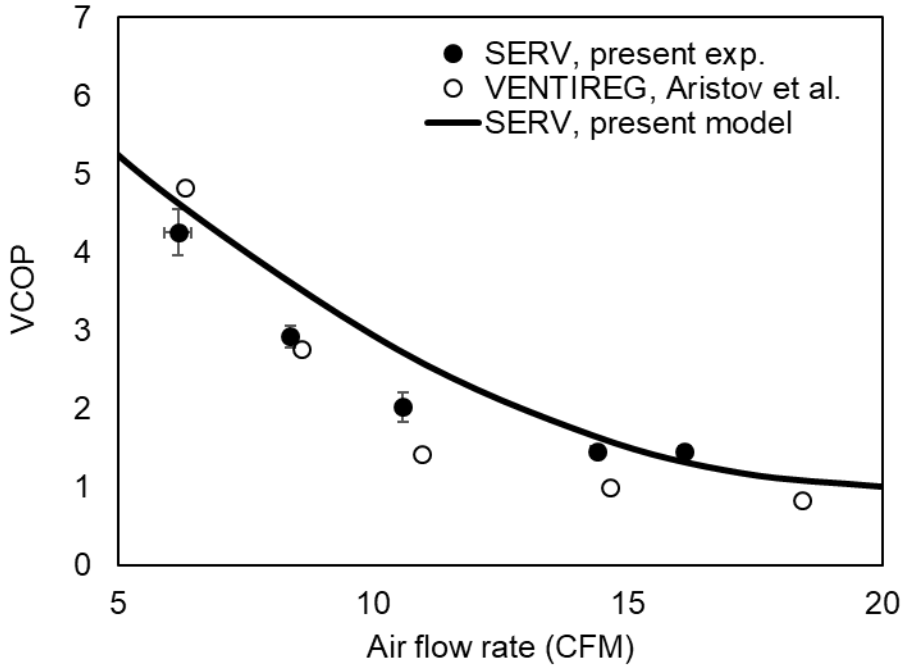

Figure 38 Comparison of VCOP of sorbent discs (SERV) to packed bed system (VENTIREG)

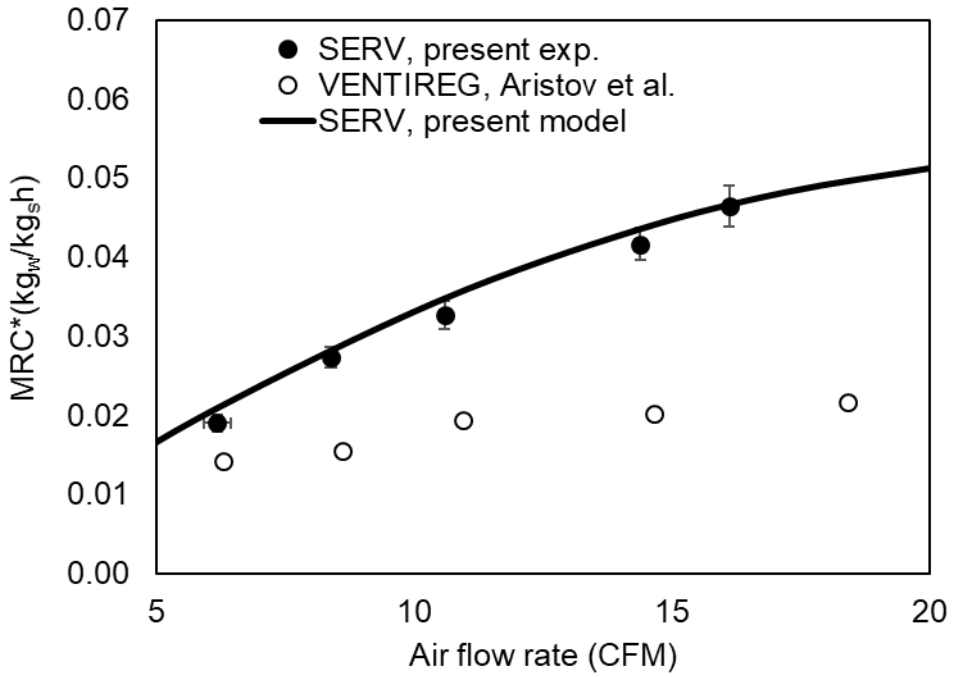

Figure 39 Comparison of MRC* of sorbent discs (SERV) to packed bed system (VENTIREG)

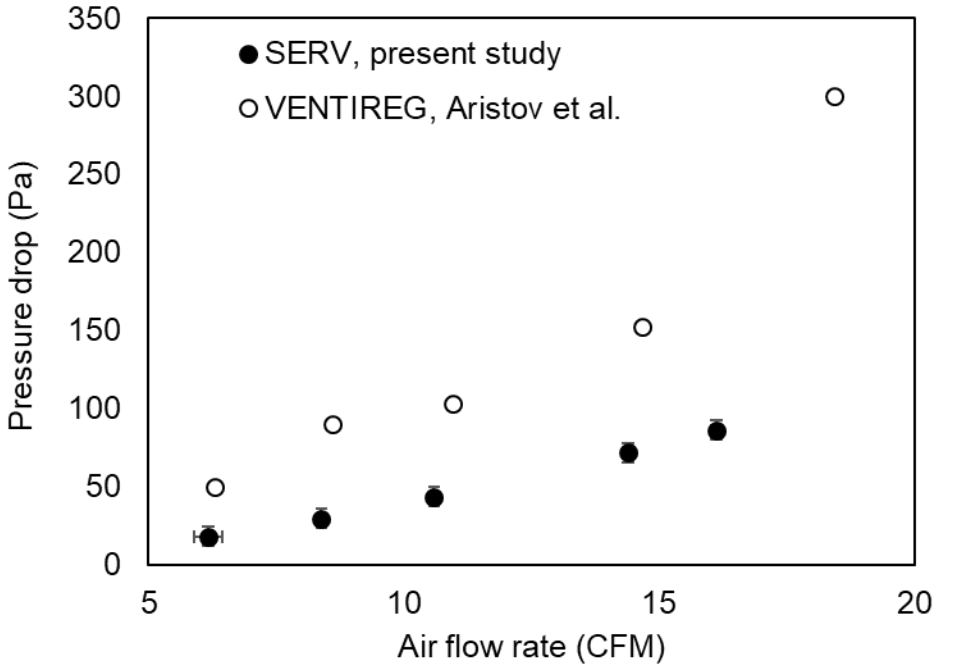

Figure 40 Comparison of pressure drop of sorbent discs (SERV) to packed bed system (VENTIREG)

Latent effectiveness, ε_L, is the nondimensionalized form of the water vapor recovery, relative to the humidity difference between humid indoor and dry outdoor conditions. Performance of the present experimental study on sorbent discs (SERV) and packed bed of $Al_2O_3/CaCl_2$ (IK-011-1) (VENTIREG) previously tested by Aristov et al. [66] is compared. At flow rates ranging from 3 to 18 CFM, both sorbent beds have similar ε_L and VCOP performance as shown in Figure 37 and Figure 38.

The compactness of the systems can be better compared by MRC^* as for sorbent discs with 2.1 kg active material and the 3 kg packed bed of $Al_2O_3/CaCl_2$ (IK-011-1). As shown in Figure 39, the MRC^* of sorbent discs (SERV) is up to 30% higher than that of the packed bed (VENTIREG) of $Al_2O_3/CaCl_2$ (IK-011-1). It means that sorbent discs have similar water sorption performance as indicated by $\varepsilon_{L,}$ however, the sorbent discs design is more compact with about 30% less sorbent mass. Considering 50 to 70% lower pressure drop as seen in Figure 40, air channeled sorbent discs is a promising design for a scaled-up system that requires less fan power.

Chapter 5. Conclusions and future work

In the context of this thesis, a proof of concept air channeled sorbent discs-based enthalpy recovery ventilation system (SERV) was proposed as a potential replacement for pertinent heat or enthalpy recovery ventilators (HRV/ERV) that require defrosting mechanisms. A theoretical model was developed to investigate the heat and mass transfer enhancement effect of developing boundary layer in air channeled sorbent discs. The sorbent discs were built and tested in a custom-built experimental set-up in our laboratory. The performance of the system was evaluated for several air flow rates, cycle times and outdoor air conditions. Main contributions resulted from the present study are listed below:

- A novel theoretical model for heat and mass transfer in air channels of sorbent discs is developed. This model can be easily implemented for investigating both the fully developed or developing flow regimes in different channel shapes.
- An air channeled sorbent disc preparation procedure is developed experimentally.
- The air channeled sorbent discs built and tested for the first time for the SERV at several different air flow rates (up to 20 CFM), cycle times and outdoor air conditions down to -15°C.
- For the tested conditions, the sorbent discs based SERV can recover up to 70% heat and 80% moisture which is in the similar range compared to the packed bed system VENTIREG, however the SERV offer 60% less pressure drop and 30% less active material.

Future work

- The novel sorbent discs design may be tested for various moisture removal applications at highly humid conditions, i.e. greenhouse air conditioning
- Mechanical properties of the composite disc should be studied for higher air flow rates
- Durability study should be performed and the effect of moisture uptake on mechanical properties should be examined
- Different channel shapes and suitable manufacturing methods, i.e. 3D printing, can be investigated for further enhancement

References

[1] H. Karunathilake, K. Hewage, and R. Sadiq, “Opportunities and challenges in energy demand reduction for Canadian residential sector: A review,” *Renew. Sustain. Energy Rev.*, vol. 82, no. February 2017, pp. 2005–2016, 2018.

[2] “Canada’s Secondary Energy Use (Final Demand) by Sector, End Use and Subsector | Natural Resources Canada.” [Online]. Available: http://oee.nrcan.gc.ca/corporate/statistics/neud/dpa/showTable.cfm?type=HB&sector=aaa&juris=ca&rn=2&page=0. [Accessed: 14-Feb-2019].

[3] “Residential Sector Canada Table 2: Secondary Energy Use and GHG Emissions by End-Use | Natural Resources Canada.” [Online]. Available: http://oee.nrcan.gc.ca/corporate/statistics/neud/dpa/showTable.cfm?type=CP&sector=res&juris=ca&rn=2&page=4. [Accessed: 14-Feb-2019].

[4] T. Kovesi *et al.*, “Indoor air quality and the risk of lower respiratory tract infections in young Canadian Inuit children.,” *CMAJ*, vol. 177, no. 2, pp. 155–60, Jul. 2007.

[5] A. ASHRAE, “ASHRAAE 62.1-2015 Ventilation for Acceptable Indoor Air Quality,” *Am. Soc. Heating, Refrig. Air Cond. Eng.*, 2015.

[6] M. Orme, “Estimates of the energy impact of ventilation and associated financial expenditures,” *Energy Build.*, vol. 33, no. 3, pp. 199–205, 2001.

[7] “ASHRAE Standard 55 Thermal Environmental Conditions for Human Occupancy,” 2010.

[8] A. Mardiana-Idayu and S. B. Riffat, “Review on heat recovery technologies for building applications,” *Renew. Sustain. Energy Rev.*, vol. 16, no. 2, pp. 1241–1255, Feb. 2012.

[9] C. Beattie, P. Fazio, R. Zmeureanu, and J. Rao, “Experimental study of air-to-air heat exchangers for use in arctic housing,” *Appl. Therm. Eng.*, vol. 129, pp. 1281–

1291, 2018.

[10] Y. I. Aristov, I. V. Mezentsev, and V. A. Mukhin, “A new approach to regenerating heat and moisture in ventilation systems,” *Energy Build.*, vol. 40, no. 3, pp. 204–208, 2008.

[11] E. Cerrah and M. Bahrami, “Optimum Performance Definition for Desiccant Wheel Systems,” in *Innovative Materials for Processes in Energy Systems (IMPRES)*, 2016, vol. 1, no. 778, pp. 102–103.

[12] E. Cerrah and M. Bahrami, “Performance Evaluation of a Novel Sorbent Based Enthalpy Recovery Ventilator in Northern Climates.”

[13] E. Cerrah, C. Mccague, and M. Bahrami, “Air-channel composite desiccant for northern climate humidity recovery ventilation system,” in *Heat Powered Cycles Conference*, 2018, vol. 2, no. 1, pp. 2–9.

[14] C. Mccague, S. Shokoya, E. Cerrah, and M. Bahrami, “Hygroscopic salts in porous matrices : Thermophysical properties and lab-scale testing for air conditioning applications.”

[15] M. Friedlander *et al.*, “ANSI/ ASHRAE Standard 84 -2013 Method of Testing Air-to-Air Heat / Energy Exchangers,” Atlanta/ USA, 2013.

[16] E. Cerrah and M.Bahrami, “A Novel Sorbent Based Enthalpy Recovery Ventilator,” in *Pacific Rim Thermal Engineering Conference (PRTECH2019)*.

[17] R. Pichs-Madruga *et al.*, “Climate Change 2014 Mitigation of Climate Change Summary for Policymakers Technical Summary Part of the Working Group III Contribution to the Fifth Assessment Report of the Intergovernmental Panel on Climate Change,” 2015.

[18] P. Nejat, F. Jomehzadeh, M. M. Taheri, M. Gohari, and M. Z. Abd. Majid, “A global review of energy consumption, CO2 emissions and policy in the residential sector (with an overview of the top ten CO2 emitting countries),” *Renew. Sustain. Energy*

Rev., vol. 43, pp. 843–862, Mar. 2015.

[19] International Energy Agency, “Energy Technology Perspectives 2016,” 2016.

[20] J. Laustsen, “Energy Efficiency Requirements in Building Codes , Energy Efficiency Policies for New Buildings,” 2008.

[21] I. - International Energy Agency, “Insights Series 2018: Energy Efficiency Potential in Canada.”

[22] Y. Somuncu and M. Pınar Menguc, “Brief Discussion of Energy Certification Systems for Buildings,” in *SBE 16*, 2016.

[23] “Climate zones—windows, doors and skylights | Natural Resources Canada.” [Online]. Available: http://www.nrcan.gc.ca/energy/products/categories/fenestration/13954. [Accessed: 21-May-2018].

[24] M. Justo Alonso, P. Liu, H. M. Mathisen, G. Ge, and C. Simonson, “Review of heat/energy recovery exchangers for use in ZEBs in cold climate countries,” *Build. Environ.*, vol. 84, pp. 228–237, 2015.

[25] ANSI/ASHRAE, “ASHRAE Standard 62.2 - 2013 Ventilation for Acceptable Indoor Air Quality,” 2013.

[26] B. of B. H. Homeowner Protection Office, “Heat Recovery Ventilation Guide for Houses,” 2015.

[27] P. Liu, M. Justo Alonso, H. M. Mathisen, and C. Simonson, “Energy transfer and energy saving potentials of air-to-air membrane energy exchanger for ventilation in cold climates,” *Energy Build.*, vol. 135, pp. 95–108, Jan. 2017.

[28] A. S. Binghooth and Z. A. Zainal, “Performance of desiccant dehumidification with hydronic radiant cooling system in hot humid climates,” *Energy Build.*, vol. 51, pp. 1–5, Aug. 2012.

[29] T. S. Ge, Y. Li, R. Z. Wang, and Y. J. Dai, “A review of the mathematical models for predicting rotary desiccant wheel,” *Renew. Sustain. Energy Rev.*, vol. 12, no. 6, pp. 1485–1528, 2008.

[30] N. Enteria, K. Mizutani, Y. Monma, T. Akisaka, and N. Okazaki, “Experimental evaluation of the new solid desiccant heat pump system in Asia-Pacific climatic conditions,” *Appl. Therm. Eng.*, vol. 31, no. 2–3, pp. 243–257, Feb. 2011.

[31] Y. Zhao, T. S. Ge, Y. J. Dai, and R. Z. Wang, “Experimental investigation on a desiccant dehumidification unit using fin-tube heat exchanger with silica gel coating,” *Appl. Therm. Eng.*, vol. 63, no. 1, pp. 52–58, Feb. 2014.

[32] C. H. Chen, C. Y. Hsu, C. C. Chen, and S. L. Chen, “Silica gel polymer composite desiccants for air conditioning systems,” *Energy Build.*, vol. 101, pp. 122–132, 2015.

[33] C. H. Chen, C. Y. Hsu, C. C. Chen, Y. C. Chiang, and S. L. Chen, “Silica gel/polymer composite desiccant wheel combined with heat pump for air-conditioning systems,” *Energy*, vol. 94, pp. 87–99, 2016.

[34] R. Narayanan, W. Y. Saman, S. D. White, and M. Goldsworthy, “Comparative study of different desiccant wheel designs,” *Appl. Therm. Eng.*, vol. 31, no. 10, pp. 1613–1620, 2011.

[35] A. Yadav and V. K. Bajpai, “Mathematical Model for Design Parameter Analysis to Improve the Performance of a Desiccant Wheel,” *Chem. Eng. Technol.*, vol. 35, no. 9, pp. 1617–1625, 2012.

[36] L. Yadav, A. Yadav, V. Dabra, and A. Yadav, “Effect of desiccant isotherm on the design parameters of desiccant wheel,” *Heat Mass Transf. und Stoffuebertragung*, vol. 50, no. 1, pp. 1–12, 2014.

[37] S. De Antonellis, C. M. Joppolo, and L. Molinaroli, “Simulation, performance analysis and optimization of desiccant wheels,” *Energy Build.*, vol. 42, no. 9, pp.

1386–1393, 2010.

[38] J. D. Chung, D. Y. Lee, and S. M. Yoon, “Optimization of desiccant wheel speed and area ratio of regeneration to dehumidification as a function of regeneration temperature,” *Sol. Energy*, vol. 83, no. 5, pp. 625–635, 2009.

[39] X. J. Zhang, Y. J. Dai, and R. Z. Wang, “A simulation study of heat and mass transfer in a honeycombed rotary desiccant dehumidifier,” *Appl. Therm. Eng.*, vol. 23, no. 8, pp. 989–1003, 2003.

[40] S. Muthu, P. Talukdar, and S. Jain, “Effect of Regeneration Section Angle on the Performance of a Rotary Desiccant Wheel,” *J. Therm. Sci. Eng. Appl.*, vol. 8, no. 1, p. 11013, 2015.

[41] X. J. Zhang, Y. J. Dai, and R. Z. Wang, “A simulation study of heat and mass transfer in a honeycombed rotary desiccant dehumidifier,” *Appl. Therm. Eng.*, vol. 23, no. 8, pp. 989–1003, 2003.

[42] H. Geun, S. Il, and S. Park, “Numerical study on heat and mass transfer in hygroscopic rotor during sorption process,” *Heat Mass Transf.*, vol. 53, no. 2, pp. 591–609, 2017.

[43] L. A. Sphaier and W. M. Worek, “Analysis of heat and mass transfer in porous sorbents used in rotary regenerators,” *Int. J. Heat Mass Transf.*, vol. 47, no. 14–16, pp. 3415–3430, 2004.

[44] C. R. Ruivo, J. J. Costa, and A. R. Figueiredo, “On the behaviour of hygroscopic wheels: Part I - channel modelling,” *Int. J. Heat Mass Transf.*, vol. 50, no. 23–24, pp. 4812–4822, 2007.

[45] T. S. Ge, F. Ziegler, and R. Z. Wang, “A mathematical model for predicting the performance of a compound desiccant wheel (A model of compound desiccant wheel),” *Appl. Therm. Eng.*, vol. 30, no. 8–9, pp. 1005–1015, 2010.

[46] Y. . Dai, R. . Wang, and H. . Zhang, “Parameter analysis to improve rotary desiccant

dehumidification using a mathematical model," *Int. J. Therm. Sci.*, vol. 40, no. 4, pp. 400–408, 2001.

[47] A. Pesaran and A. Mills, "Moisture transport in silica gel packed beds - II. Experimental study," *Int. J. Heat Mass Transf.*, vol. 30, no. 6, pp. 1037–1049, 1987.

[48] P. L. Brillhart, "Evaluation of desiccant rotor matrices using an advanced fixed-bed test system.," University of Illinois at Chicago, 1997.

[49] F. Incropera, D. DeWitt, and T. Bergrnan, *Fundamentals of Heat and Mass Transfer (The 6th Edition)*, 6th ed. 2007.

[50] C. R. Ruivo, J. J. Costa, and A. R. Figueiredo, "On the validity of lumped capacitance approaches for the numerical prediction of heat and mass transfer in desiccant airflow systems," *Int. J. Therm. Sci.*, vol. 47, no. 3, pp. 282–292, 2008.

[51] C. J. Simonson and R. W. Besant, "Heat and Moisture Transfer in Desiccant Coated Rotary Energy Exchangers : Part I . Numerical Model," *HVAC&R Res.*, vol. 3, no. 4, pp. 325–350, 1997.

[52] G. Angrisani, C. Roselli, and M. Sasso, "Effect of rotational speed on the performances of a desiccant wheel," *Appl. Energy*, vol. 104, pp. 268–275, 2013.

[53] C. X. Jia, Y. J. Dai, J. Y. Wu, and R. Z. Wang, "Use of compound desiccant to develop high performance desiccant cooling system," *Int. J. Refrig.*, vol. 30, no. 2, pp. 345–353, 2007.

[54] L. A. Sphaier and W. M. Worek, "Analysis of heat and mass transfer in porous sorbents used in rotary regenerators," *Int. J. Heat Mass Transf.*, vol. 47, no. 14–16, pp. 3415–3430, 2004.

[55] L. Yadav and A. Yadav, "Mathematical investigation of purge sector angle for clockwise and anticlockwise rotation of desiccant wheel," *Appl. Therm. Eng.*, vol. 93, pp. 839–848, 2016.

[56] M. Intini, M. Goldsworthy, S. White, and C. M. Joppolo, “Experimental analysis and numerical modelling of an AQSOA zeolite desiccant wheel,” *Appl. Therm. Eng.*, vol. 80, pp. 20–30, 2015.

[57] A. A. Pesaran, A. F. M. Seri, and S. Energy, “Moisture Transport in Silica Gel Packed Beds,” vol. 30, no. 6, pp. 1037–1049, 1986.

[58] Y. S. M. and M.M.Yovanovich, “Modeling nusselt numbers for thermally developing laminar flow in non-circular ducts,” 1998.

[59] A. Tamayol and M. Bahrami, “Laminar Flow in Microchannels With Noncircular Cross Section,” *J. Fluids Eng.*, vol. 132, no. 11, p. 111201, 2010.

[60] Y. S. Muzychka and M. M. Yovanovich, “Laminar Forced Convection Heat Transfer in the Combined Entry Region of Non-Circular Ducts,” *J. Heat Transfer*, vol. 126, no. 1, p. 54, 2004.

[61] Y. S. Muzychka, M. M. Yovanovich, G. P. Celata, B. Thonon, A. Bontemps, and S. Kandlikar, “Laminar Flow Friction and Heat Transfer in Non- Circular Ducts and Channels Part I- Hydrodynamic Problem Compact Heat Exchangers Proceedings Editors,” *Compact Heat Exch. A Festschrift 60th Birthd. Ramesh K. Shah*, 2002.

[62] Y. S. M. and M. M. Yovanovich, “Laminar Flow Friction and Heat Transfer in NonCircular Ducts and Channels Part II- Thermal Problem,” *Compact Heat Exch. A Festschrift 60th Birthd. Ramesh K. Shah*, 2002.

[63] E. Sadeghi, M. Bahrami, and N. Djilali, “Estimation of nusselt number in microchannels of arbitrary cross section with constant axial heat flux,” *Heat Transf. Eng.*, vol. 31, no. 8, pp. 666–674, 2010.

[64] R. K. Shah and A. L. London, *Laminar Flow Forced Convection in Ducts: A Source Book for Compact Heat Exchanger Analytica Data*. 1978.

[65] L. Z. Zhang and J. L. Niu, “Performance comparisons of desiccant wheels for air dehumidification and enthalpy recovery,” *Appl. Therm. Eng.*, vol. 22, no. 12, pp.

1347–1367, 2002.

[66] Y. I. Aristov, I. V. Mezentsev, and V. A. Mukhin, “Investigation of the moisture exchange in a stationary adsorbent layer through which air is passed,” *J. Eng. Phys. Thermophys.*, vol. 78, no. 2, pp. 44–50, 2005.

[67] E. ISO, “5167: Measurement of Fluid Flow by Means of Pressure Differential devices,” *Int. Organ. Stand.*, vol. 2003, pp. 1–11, 2003.

[68] H. W. Coleman and W. G. Steele, *Experimentation, validation, and uncertainty analysis for engineers*. .

[69] M. Rafati Nasr, F. Fathieh, D. Kadylak, R. Huizing, R. W. Besant, and C. J. Simonson, “Experimental methods for detecting frosting in cross-flow air-to-air energy exchangers,” *Exp. Therm. Fluid Sci.*, vol. 77, pp. 100–115, Oct. 2016.

[70] International Code Council, *International mechanical code 2015*. 2015.

Appendix A.

Experimental data for different operating conditions, air flow rate, half cycle time, temperature and RH are presented in Table 11.

Table 11 Experimental data

Date	Air flow rate (CFM)	Set half cycle time (s)	Latent effectiveness	VCOP	MRC* (kg/h)	T outdoor (°C)	RH dry (%)	T dry (°C)	w dry (g/kg)	RH indoor(%)	T indoor (°C)	w indoor(g/kg)	Pressure drop (Pa)
3/14/2019	18	120	0.45	0.80	0.05	-6.7	20.1	12.4	1.78	49.8	23.0	8.69	102
3/15/2019	18	60	0.51	1.01	0.04	-5.9	29.5	12.7	2.66	49.5	21.5	7.86	102
3/15/2019	18	300	0.29	0.40	0.04	-8.0	22.1	6.9	1.66	61.9	21.0	9.59	102
3/16/2019	18	60	0.41	0.67	0.05	-12.8	43.7	11.6	3.96	64.6	23.4	11.82	102
3/16/2019	18	120	0.32	0.46	0.05	9.1	40.6	9.1	3.36	70.9	23.4	12.98	102
3/17/2019	16	120	0.34	0.52	0.03	-14.1	38.0	6.6	2.54	61.6	20.3	9.20	84

Date	Air flow rate (CFM)	Set half cycle time (s)	Latent effectiveness	VCOP	MRC* (kg/h)	T outdoor (°C)	RH dry (%)	T dry (°C)	w dry (g/kg)	RH indoor(%)	T indoor (°C)	w indoor(g/kg)	Pressure drop (Pa)
3/17/2019	16	60	0.42	0.71	0.03	-14.2	46.7	7.6	3.18	59.2	20.0	8.75	84
3/17/2019	11	60	0.49	0.93	0.02	-13.8	42.8	9.1	3.20	56.2	20.5	8.54	49
3/17/2019	11	120	0.41	0.70	0.02	-14.7	37.1	7.9	2.66	59.2	20.6	9.01	49
3/18/2019	12	300	0.31	0.45	0.03	-13.3	28.3	5.5	1.94	65.4	20.5	9.87	55
4/7/2019	9	60	0.62	3.01	0.02	-6.6	17.2	11.1	1.43	27.1	21.5	4.32	34
4/7/2019	9	120	0.52	1.06	0.01	-7.2	16.2	11.0	1.36	29.0	21.6	4.65	34
4/7/2019	9	180	0.49	0.93	0.01	-6.7	16.5	10.1	1.31	30.4	21.4	4.80	34

Date	Air flow rate (CFM)	Set half cycle time (s)	Latent effectiveness	VCOP	MRC* (kg/h)	T outdoor (°C)	RH dry (%)	T dry (°C)	w dry (g/kg)	RH indoor(%)	T indoor (°C)	w indoor(g/kg)	Pressure drop (Pa)
4/7/2019	13	60	0.62	2.71	0.02	-7.3	19.2	9.1	1.40	28.7	21.0	4.47	61
4/8/2019	6	120	0.65	0.63	0.00	-5.0	11.5	13.1	1.11	29.3	22.2	4.85	19
4/10/2019	6	300	0.59	1.43	0.01	-4.7	10.9	12.9	1.04	29.9	22.2	4.96	17
4/10/2019	6	240	0.56	1.29	0.01	-4.2	11.8	12.4	1.07	30.3	22.2	5.00	17
4/10/2019	6	180	0.58	1.37	0.01	-4.5	12.4	12.1	1.11	30.1	21.9	4.89	18
4/10/2019	6	120	0.62	1.63	0.01	-3.9	12.5	12.7	1.16	30.2	22.0	4.96	18
4/10/2019	6	60	0.83	4.72	0.01	-3.9	14.1	14.0	1.44	27.8	22.2	4.60	18

Date	Air flow rate (CFM)	Set half cycle time (s)	Latent effectiveness	VCOP	MRC* (kg/h)	T outdoor (°C)	RH dry (%)	T dry (°C)	w dry (g/kg)	RH indoor(%)	T indoor (°C)	w indoor(g/kg)	Pressure drop (Pa)
4/13/2019	10	60	0.75	2.68	0.02	-6.4	20.0	8.6	1.44	28.4	20.6	4.30	42
4/13/2019	10	120	0.51	1.08	0.01	-6.4	20.4	7.5	1.35	31.4	20.4	4.70	42
4/13/2019	10	180	0.48	0.88	0.01	-6.4	20.1	7.3	1.32	32.6	20.5	4.91	42
4/13/2019	13	60	0.69	2.00	0.02	-5.2	23.0	6.9	1.43	32.1	20.2	4.75	57
4/13/2019	13	120	0.47	0.87	0.02	-8.3	20.5	6.0	1.24	36.3	20.7	5.56	61
4/18/2019	8	60	0.73	2.56	0.01	-4.4	21.6	11.3	1.84	29.2	21.6	4.68	30
4/18/2019	17	60	0.61	1.47	0.03	-7.7	27.4	6.3	1.67	33.4	20.6	5.11	94

Date	Air flow rate (CFM)	Set half cycle time (s)	Latent effectiveness	VCOP	MRC* (kg/h)	T outdoor (°C)	RH dry (%)	T dry (°C)	w dry (g/kg)	RH indoor(%)	T indoor (°C)	w indoor(g/kg)	Pressure drop (Pa)
4/18/2019	8	60	0.74	2.81	0.02	-3.7	22.1	11.7	1.93	30.3	22.0	5.00	30
4/18/2019	8	60	0.73	2.61	0.02	-12.0	19.8	9.0	1.48	32.0	21.4	5.00	29
4/18/2019	8	60	0.69	2.13	0.01	2.0	28.5	13.1	2.68	32.1	21.9	5.20	27
4/18/2019	8	60	0.75	2.86	0.01	6.0	23.2	14.9	2.46	30.9	22.0	5.09	29
4/18/2019	8	60	0.74	2.71	0.01	9.7	27.6	16.7	3.25	31.3	22.4	5.20	29
4/18/2019	8	60	0.73	2.68	0.02	-21.2	22.1	6.7	1.44	31.8	21.4	5.00	28
4/29/2019	4	60	0.87	6.66	0.01	2.6	21.3	16.0	2.40	29.8	22.3	4.90	8

Date	Air flow rate (CFM)	Set half cycle time (s)	Latent effectiveness	VCOP	MRC* (kg/h)	T outdoor (°C)	RH dry (%)	T dry (°C)	w dry (g/kg)	RH indoor(%)	T indoor (°C)	w indoor(g/kg)	Pressure drop (Pa)
4/29/2019	6	60	0.81	4.32	0.01	-3.7	17.8	14.7	1.88	30.5	21.7	4.90	19
4/29/2019	9	60	0.72	2.53	0.02	-3.7	18.2	12.1	1.64	31.6	21.3	4.90	31
4/29/2019	3	60	0.91	9.44	0.02	1.25	20.6	17.3	2.50	30.0	22.7	5.09	6
4/29/2019	6	60	0.80	3.83	0.01	-7.9	16.7	14.1	1.70	30.7	22.1	5.07	19
4/29/2019	9	60	0.72	2.47	0.02	-11.2	16.5	10.7	1.38	31.5	21.6	5.04	32
4/30/2019	3	60	0.91	10.55	0.01	3.3	21.5	18.2	2.70	37.0	22.7	6.33	7
4/30/2019	6	60	0.81	4.25	0.02	-2.6	18.0	15.2	1.98	36.7	21.8	5.95	18

Date	Air flow rate (CFM)	Set half cycle time (s)	Latent effectiveness	VCOP	MRC* (kg/h)	T outdoor (°C)	RH dry (%)	T dry (°C)	w dry (g/kg)	RH indoor(%)	T indoor (°C)	w indoor(g/kg)	Pressure drop (Pa)
4/30/2019	8	60	0.75	2.92	0.02	-4.4	18.6	13.2	1.83	37.5	21.7	6.36	30
4/30/2019	11	60	0.68	2.02	0.03	-5.0	20.7	10.8	1.74	41.9	21.1	6.55	43
4/30/2019	14	60	0.60	1.46	0.04	-5.8	22.0	8.5	1.63	46.6	20.9	6.60	72
4/30/2019	16	60	0.60	1.46	0.04	-6.0	24.4	7.9	1.69	45.2	20.3	6.74	86
4/30/2019	8	60	0.74	2.71	0.03	-4.1	19.6	12.8	1.87	43.4	21.6	6.97	29
5/2/2019	6	60	0.83	4.57	0.01	-2.0	20.2	14.8	2.15	31.6	21.7	5.08	19
5/2/2019	6	120	0.63	1.68	0.01	-2.1	17.2	12.9	1.62	34.2	21.6	5.48	18

Date	Air flow rate (CFM)	Set half cycle time (s)	Latent effectiveness	VCOP	MRC* (kg/h)	T outdoor (°C)	RH dry (%)	T dry (°C)	w dry (g/kg)	RH indoor(%)	T indoor (°C)	w indoor(g/kg)	Pressure drop (Pa)
5/2/2019	6	180	0.60	1.51	0.01	-2.3	15.7	13.0	1.49	34.9	21.7	5.62	18
5/2/2019	6	240	0.59	1.39	0.01	-2.2	14.7	13.0	1.41	35.2	21.8	5.69	18
5/2/2019	6	300	0.57	1.32	0.01	-2.3	14.1	13.1	1.35	34.4	22.0	5.81	18
5/2/2019	6	60	0.79	3.85	0.01	-0.8	19.8	14.4	2.05	31.4	22.0	5.15	18

Appendix B.

The Matlab code presented in this section is to model the heat and mass transfer in sorbent disc air channels.

```
%% Sorbent discs heat and mass transfer model

clear
clc
%% %%%%%%%%%%%%%%%%%%%%%%%%%%%%%%%%%%%%%%%%%%%%%%%%%%%%%%%%%%%%%%%%
%%%%%%%%%%%%%%%% Design Parameters %%%%%%%%%%%%%%%%
%%%%%%%%%%%%%%%%%%%%%%%%%%%%%%%%%%%%%%%%%%%%%%%%%%%%%%%%%%%%%%%%%%%

cycle_time = 120; %s, cycle time
t_pro = 60; %s, exhale period
t_rg = 60; %s, inhale period
number_of_discs = 5;
thickness = 0.025*number_of_discs; %m, for each disc 25 mm thick
D_overall=0.2032 ;    %m, wheel diameter

% Channel geometry
d = 0.000;  %m, channel diameter
delta = 0.0085;  %wall thickness , m
a= d + 2*delta;  %m
b= d + 2*delta; %m

aspect_ratio = a/b;

P = pi * d; %m, perimeter

area_crosssection = (pi*(d^2)/4); %crosssection of the channel, m^2
A_d = (pi*(a^2)/4) - (pi*(d^2)/4); %sorbent wall cross sectional area,
m^2
d_h= area_crosssection^0.5;   %characteristic length

u0 = 3; %air velocity in the channel, m/s

%%%%%%%%%%%%%%%%%%%%%%%%%%%%%%%%%%%%%%%%%%%%

T_ambient = 22.83; %degree C, room return temperature
w_ambient = 0.0086; %kg/kg, room return specific humidity

P_total = 101325;  % atmospheric pressure, Pa

Td_0 = 22;              %degree C, initial sorbent temperature
T_0 = 22;               %degree C, initial air temperature
w_0 = 0.004152;         %kg/kg, initial air humidity ratio
Wd_0 = 0.2;             %kg/kg, initial uptake value

u_ad = u0;
```

```
T_ad = T_ambient;
w_ad = w_ambient;
u_rg = u0;
T_rg = 13; % sensible effectiveness for outdoor -10C
%[degree C]
w_rg = 0.001; %0.000837; %0.00165; %0.0182;
u_in = u_ad;
T_in = T_ad;              % [degree C]
w_in = w_ad;           % humidity ratio

%% %%%%%%%%%%%%%%%%%%%%%%%%%%%%%%%%%%%%%%%%%%%%%%%%%%%%%%%%%%%%%%%%%%%%%%%%
%%%%%%%%%%%%%%%% Solution Parameters %%%%%%%%%%%%%%%%
%%%%%%%%%%%%%%%%%%%%%%%%%%%%%%%%%%%%%%%%%%%%%%%%%%%%%%%%%%%%%%%%%%%%%%%%%%

N = 60; %number of discrete units
t = 0;                          % [s]
t_end =  cycle_time * 12;    % [s]         % total running time
dz = thickness / (N);
dt = 0.0001;                 % [s], time step


w = zeros (N,1);
wd = zeros (N,1);
T = zeros (N,1);
Td = zeros (N,1);
Wd = zeros (N,1);

Q_adt= zeros (N,1);
d_WA = zeros (N,1);
d_TA = zeros (N,1);
Res = zeros (4*N,1);
u_rk = zeros (4*4*N,1);


%% %%%%%%%%%%%%%%%%%%%%%%%%%%%%%%%%%%%%%%%%%%%%%%%%%%%%%%%%%%%%%%%%%%%%%%%%
%%%%%%%%%%%%%%%% Material Properties %%%%%%%%%%%%%%%%%
%%%%%%%%%%%%%%%%%%%%%%%%%%%%%%%%%%%%%%%%%%%%%%%%%%%%%%%%%%%%%%%%%%%%%%%%%%

air_density = 1.186;              % kg / m^3
adsorbent_density = 720;          % kg / m^3
bed_density = adsorbent_density;

mu_air = 1.7*10^-5;
```

```
%% %%%%%%%%%%%%%%%%%%%%%%%%%%%%%%%%%%%%%%%%%%%
%%%%%%%%%% Initial and Boundary Conditions %%%%%%%%%%
%%%%%%%%%%%%%%%%%%%%%%%%%%%%%%%%%%%%%%%%%%%%%%%%%%%%%%%

w (:)= w_0;
T (:)= T_0;
Td (:)= Td_0;
Wd (:)= Wd_0;


WriteFile =
[0,0,0,0,0,0,0,0,0,0,0,0,0,0,0,0,0,0,0,0,0,0,0,0,0,0,0,0,0,0,0,0,0,0,0,0,0,0,
0,0,0,0,0,0];

%% %%%%%%%%%%%%%%%%%%%%%%%%%%%%%%%%%%%%%%%%%%%
%%%%%%%%%% Heat and Mass Transfer Coefficients %%%%%%%%%%
%%%%%%%%%%%%%%%%%%%%%%%%%%%%%%%%%%%%%%%%%%%%%%%%%%%%%%%

Re = air_density*u_in*d_h/mu_air;
k_a = 0.0263; %W/mK
ro_a = air_density;
Re = ro_a*u_in*d_h/mu_air;
Pr_air = 0.707;
entry_length = 0.05*Re*Pr_air*d_h;  %number if Gr<20 radial temperature
profile is fully developed

%% Yovanovich constants
c_2 = 1;
c_1T = 3.01;
c_3T = 0.409;

c_1H = 3.66;
c_3H = 0.501;

gamma = 1/10; %gamma high

hyd_entry_length_yova = 0.0822*aspect_ratio*(1+aspect_ratio)^2 * ( 1-
(192*aspect_ratio*tanh(pi/(2*aspect_ratio)))/(pi^5) )^2 ;   % ref.
Laminar Flow Friction and Heat Transfer in Non-Circular Ducts and
Channels Part IHydrodynamicProblem
therm_entry_length_yovaT = 19.8*(c_2*c_3T/c_1T)^3 *
aspect_ratio^(1+3*gamma) * (1+aspect_ratio)^2 * ( 1-
(192*aspect_ratio*tanh(pi/(2*aspect_ratio)))/(pi^5) )^2 ; % ref.
Laminar Flow Friction and Heat Transfer in Non-Circular Ducts and
Channels Part II ThermalProblem
therm_entry_length_yovaH = 19.8*(c_2*c_3H/c_1H)^3 *
aspect_ratio^(1+3*gamma) * (1+aspect_ratio)^2 * ( 1-
(192*aspect_ratio*tanh(pi/(2*aspect_ratio)))/(pi^5) )^2 ; % ref.
Laminar Flow Friction and Heat Transfer in Non-Circular Ducts and
Channels Part II ThermalProblem

hydraudynamic_entry_length = thickness/(25*d_h*Re);
```

```
hydraudynamic_entry_length_chen = d_h * ( 0.6/(0.035*Re+1) + 0.056*Re
);

%for fully developed flow, calculated by the analytical model code
Nu_Hfd = 3.86;
Nu_Tfd = 3.24;
Nu_fd = (Nu_Hfd + Nu_Tfd)/2;
%for developing flow, calculated by the analytical model code
Nu_Hd = 188.56;
Nu_Td = 136.43;
Nu_d = (Nu_Hd + Nu_Td)/2;

Nu = Nu_d;
                h = Nu * k_a / d_h;  % convective heat transfer
coefficient

                 cp_a = 1009; %J/kgK
                  hm = h / (cp_a); % convective mass transfer
coefficient  ro_a should not be there   does not change if it is ca


%% %%%%%%%%%%%%%%%%%%%%%%%%%%%%%%%%%%%%%%%%%%%%%%%%%%%%%%%%%%%%%%%%
%%%%%%%%%%%%%%%%%%%% Solution %%%%%%%%%%%%%%%%%%%%%%%%%%%%%%%%%%%%
%%%%%%%%%%%%%%%%%%%%%%%%%%%%%%%%%%%%%%%%%%%%%%%%%%%%%%%%%%%%%%%%%

w0=w_ambient;
T0=T_ambient;
P0=P_total;

l = 0;
counter=0;
 while t < t_end
    for j = 0:2

            remain = rem (t,(cycle_time));


        for i = 2 : N-1
            d_WA (i) = ( w (i+1) - w (i-1) ) / ( 2.0 * dz );
        end


        for i = 2 : N-1
            d_TA (i) = ( T (i+1) - T (i-1) ) / ( 2.0 * dz );
        end


     if (0<=remain && remain<= t_pro)


        d_WA (1) = ( 0.5*(w (2)+w(1)) - w_ad ) / (dz);
        d_WA (N) = ( w (N) - w (N-1) ) / dz;
```

```
        d_TA (1) = ( 0.5*(T (2)+T(1)) - T_ad ) / (dz);
        d_TA (N) = ( T (N) - T (N-1) ) / dz;

         else


        d_WA (1) = ( w (2) - w (1) ) / dz;
        d_WA (N) = (w_rg- 0.5*(w (N)+w(N-1)) ) / (dz);

        d_TA (1) = ( T (2) - T (1) ) / dz;
        d_TA (N) = ( T_rg  - 0.5*(T (N)+T(N-1)) ) /(dz);
    end

        [Wd, Td, wd] = isotherm (N, P_total, Wd, Td,wd);

         Sh = Nu;


        for i = 1 : N
            air_mass_flow_rate = air_density * u_in *
area_crosssection;
            ca = 1000*(1.884 * w (i) + 1.005 * (1.0 - w (i))); %J/kg
            cb = 1000*(4.178 * Wd (i) + 0.921);           % J/kg

            if (Wd (i) <= 0.05)                           %
                Q_ad = 1000*(-12400 * Wd (i) + 3500);  %J/kg, heat of
adsorption
            else
                Q_ad = 1000*(-1400 * Wd (i) + 2950);
            end


            %%%%%%%%%%%%%%%%%%%%%%%%%%%%%%%%%%%%%%%%%%%%%%%%%%%%%%%%%


%% CONSERVATION EQUATIONS

            % Moisture Transport in gas phase (w)
            Res (0*N+i) = -
((air_mass_flow_rate/(air_density*area_crosssection)) * d_WA (i)) - (hm
* (P /( area_crosssection*air_density)) * ( w (i) - wd (i) ))   ;

            % Moisture Transport in solid phase (Wd)
            Res (1*N+i) = (hm*P/(bed_density* A_d))   * ( w (i) - wd (i)
);

            % Heat Transfer in gas phase (T)
            Res (2*N+i) = -(air_mass_flow_rate
/(air_density*area_crosssection)) * d_TA (i) +
```

```
((P/(air_density*area_crosssection*ca)) * ( -2* h ) * ( T (i) - Td (i)
));  %cp_v*hm * ( w (i) - wd (i) )

            % Heat Transfer in solid phase (Td)
            Res (3*N+i) = (Q_ad /cb)*Res (1*N+i) - ((h *P/(cb *
bed_density * A_d)) * ( Td (i) - T (i) ));
        end


        [w,Res, u_rk] = RungeKuttaStep(N,j,0,dt,w,Res,u_rk);
        [Wd,Res, u_rk] = RungeKuttaStep(N,j,1,dt,Wd,Res,u_rk);
        [T,Res, u_rk] = RungeKuttaStep(N,j,2,dt,T,Res,u_rk);
        [Td,Res, u_rk] = RungeKuttaStep(N,j,3,dt,Td,Res,u_rk);


    end

    remain = rem (t,(cycle_time));


    t = t + dt;
    l = l+1;
    if (0<=remain && remain<= t_pro)

         u_in = u_ad;
    else
        u_in = -u_rg;

    end

     steady = (t_end/cycle_time)-1;
     current = t/cycle_time;
     if current > steady
        if (rem (l,1/dt)==0)
         WriteFile =[WriteFile ; [t,
Td(1,1),Td(2,1),Td(3,1),Td(4,1),Td(5,1),Td(6,1),Td(7,1),Td(8,1),Td(9,1)
,Td(N,1),T(1,1),T(2,1),T(3,1),T(4,1),T(5,1),T(6,1),T(7,1),T(8,1),T(9,1)
,T(N,1),
Wd(1,1),Wd(2,1),Wd(3,1),Wd(4,1),Wd(5,1),Wd(6,1),Wd(7,1),Wd(8,1),Wd(9,1)
,Wd(N,1),w(1,1),w(2,1),w(3,1),w(4,1),w(5,1),w(6,1),w(7,1),w(8,1),w(9,1)
,w(N,1)]];

        end
     end
 end


xlswrite('u3_5discs_10cfm_60s_D8d5_69ch.xlsx', WriteFile);
```

Appendix C.

The Matlab code presented in this section is the analytical model that is used to calculate the Nusselt number for both the entry region and the fully developed region.

```
%% Nusselt calculation for circular channel
%Reference model: Muzychka, Y. S., & Yovanovich, M. (1998). Modeling
Nusselt numbers for thermally developing laminar flow in non-circular
ducts. In 7th AIAA/ASME Joint Thermophysics and Heat Transfer
Conference (p. 2586)[58].

%channel geometry
d = 5*10^-3;
delta = 0.011/2; %m
a = d+2*delta;
b = d+2*delta;

disk_thickness = 0.025;

 angle = pi/4;  %for similarity to triangle

A_cs = pi*d^2/4; %cross sectional area

A_rec = a*b;
A_triangle = a* b / 2;
del_rec = abs(1-A_cs/A_rec) ;
del_tri = abs(1-A_cs/A_triangle);
del = del_rec - del_tri;  %del>0.2 lower model;  del<-0.2 upper model
and del in between is middle model

epsilon = b /a;  %aspect ratio

g_eps = ( (1.086957^(1-epsilon)) * (epsilon^0.5-epsilon^1.5)+epsilon)^-
1 ;
fRe = 8*(pi^0.5)*g_eps;

charac_length = A_cs^0.5;

P_w = pi*a; %wet perimeter
porosity_cell = (pi*(d^2)/4)/(a*b);

Flow_rate =14.8; %m3/h
D = 0.1524; %m, disc diameter
total_area = pi*(D^2)/4;

F_m = (Flow_rate/3600)/total_area; %%m3/sm2
u_in = 2.5; %F_m / porosity_cell;

% Fully developed
```

```
gamma_high = 1/10;  %defines upper bound for rectangular or elliptic
duct
gamma_low = -3/10;  %defines the lower bound such as triangle,sine


Nu_rootA_H = 3.86 * (fRe / (8*(pi^0.5)*epsilon^gamma_high));
%Trapezoid fully developed cst heat flux  compare this with
Dr.Bahrami's
Nu_rootA_T = 3.24 * (fRe / (8*(pi^0.5)*epsilon^gamma_high));
%Trapezoid fully developed cst T

%% Entrance region general model for both hydrodynamic and thermally
developing flow
% Laminar Forced Convection Heat Transfer in the Combined Entry Region
of
% Non-Circular Ducts 2004 Yovanovich

C1 = 1; %average
C2_T = 0.409;
C2_H = 0.501;

C3_T = 3.01;
C3_H = 3.66;

mu_air = 1.7*10^-5;

ro_a = 1.186;
Pr_air = 0.707;

Re_L = ro_a*u_in*charac_length/mu_air;

hydr_entrance_length = 0.9308 * epsilon * (( (ellipticE ((1-
epsilon^2)^0.5)) / (1+epsilon^2) )^2) * charac_length * Re_L ;

L_th = 49.736 * (epsilon^(2+3*gamma_high) ) * ((C1*C2_T/C3_T)^3) * ((
(ellipticE ((1-epsilon^2)^0.5)) / (1+epsilon^2) )^2) * charac_length *
Re_L * Pr_air;
z_ = disk_thickness / (charac_length * Re_L * Pr_air);


m = 2.27+1.65*Pr_air^(1/3);
f_Pr_T = 0.564/ ((1+(1.664*Pr_air^(1/6))^(9/2))^(2/9));
f_Pr_H = 0.886/ ((1+(1.909*Pr_air^(1/6))^(9/2))^(2/9));

C1_bH = 3.86;
C1_bT = 3.24;

C3_bH = 0.501;
C3_bT = 0.409;

C2_b = 1; %local
C4_b = 1; %local
```

```
gamma_high = 1/10;  %defines the upper bound such as trapezoid,
rectangle, elliptic duct
gamma_low = -3/10;  %defines the lower bound such as triangle,sine
gamma_middle = (gamma_high + gamma_low)/2;


for i=1:100
dz = 0.004/100;
z(i)=i*dz;

Nu_rootA_H_dev(i) = (
(C4_b*f_Pr_H/((z(i)/(charac_length*Re_L*Pr_air))^0.5))^m +  (
(C2_b*C3_bH*(fRe/(z(i)/(charac_length*Re_L*Pr_air)))^(1/3))^5 +
(C1_bH*(fRe/(8*(pi^0.5)*epsilon^gamma_high)))^5) ^(m/5) )^(1/m);

Nu_rootA_T_dev(i) = (
(C4_b*f_Pr_T/((z(i)/(charac_length*Re_L*Pr_air))^0.5))^m +  (
(C2_b*C3_bT*(fRe/(z(i)/(charac_length*Re_L*Pr_air)))^(1/3))^5 +
(C1_bT*(fRe/(8*(pi^0.5)*epsilon^gamma_high)))^5) ^(m/5) )^(1/m);

Nu_H_dev(1)=0;
Nu_H_dev(i+1) = dz*Nu_rootA_H_dev(i) + Nu_H_dev(i);
Nu_H_dev_mean = Nu_H_dev(i+1)/0.004;

Nu_T_dev(1)=0;
Nu_T_dev(i+1) = dz*Nu_rootA_T_dev(i) + Nu_T_dev(i);
Nu_T_dev_mean = Nu_T_dev(i+1)/0.004;

end

fRe_Asq = ( ( 12/( (epsilon^0.5)*(1+epsilon)*( 1-
192*(epsilon/pi^5)*tanh(pi/(2*epsilon)) )  ) )^2 + (3.44/(z_^(1/2)))^2
)^(1/2);
```